TITLE

Members of the CUGBP Elav-Like Family of RNA-Binding Proteins are Expressed in Distinct Populations of Primary Sensory Neurons

AUTHORS

Eliza Grlickova-Duzevik[1,2] egrlickovaduzevik@une.edu
Thomas M Reimonn[4] Thomas.Reimonn@umassmed.edu
Merilla Michael[1,2] merilla.michael@gmail.com
Tina Tian[5,6,7] tina.tian@emory.edu
Jordan Owyoung[7,8] jordan.nicole.owyoung@emory.edu
Aidan McGrath-Conwell[2,3] amcgrathconwell@une.edu
Peter Neufeld[2,3] pneufeld@une.edu
Madison Mueth[2,9] mmueth@une.edu
Derek C Molliver[1,2] dmolliver@une.edu
Patricia Jillian Ward[6,7] jill.ward@emory.edu
Benjamin J Harrison[1,2] bharrison2@une.edu

1. Biomedical Sciences, College of Osteopathic Medicine, University of New England, Biddeford. ME 04005
2. Center for Excellence in the Neurosciences, University of New England. ME 04005
3. College of Arts and Sciences, University of New England, Biddeford. ME 04005
4. University of Massachusetts Medical School, Program in Bioinformatics and Integrative Biology, Worcester, MA
5. Medical Scientist Training Program, Emory University, Atlanta, GA
6. Neuroscience Graduate Program, Emory University, Atlanta, GA
7. Emory University School of Medicine, Department of Cell Biology, Atlanta, GA
8. Genetics and Molecular Biology Graduate Program, Atlanta, GA
9. Graduate School of Biomedical Science and Engineering, University of Maine, Orono, ME 04469

ACKNOWLEDGMENTS:

P20GM103643 MH116492 T32GM107000

ABSTRACT

Primary sensory Dorsal Root Ganglia (DRG) neurons are diverse, with distinct populations that respond to specific stimuli. Previously, we observed that functionally distinct populations of DRG neurons express mRNA transcript variants with different 3' untranslated regions (3'UTR's). 3'UTRs harbor binding sites for interaction with RNA-binding proteins (RBPs) for transporting mRNAs to subcellular domains, modulating transcript stability and regulating the rate of translation. In the current study, analysis of publicly available single-cell RNA-Sequencing (scRNA-Seq) data generated from adult mice revealed that 17 3'UTR-binding RBPs were enriched in specific populations of DRG neurons. This included 4 members of the CUGBP Elav-Like Family (CELF): CELF2 and CELF4 were enriched in peptidergic, CELF6 in both peptidergic and nonpeptidergic and CELF3 in tyrosine hydroxylase-expressing neurons. Immunofluorescence studies confirmed that 60% of CELF4+ neurons are small diameter C fibers and 33% medium diameter myelinated (likely Aδ) fibers and showed that CELF4 is distributed to peripheral termini. Co-expression analyses using transcriptomic data and immunofluorescence revealed that CELF4 is enriched in nociceptive neurons that express GFRA3, CGRP and the capsaicin receptor TRPV1. Re-analysis of published transcriptomic data from macaque DRG revealed a highly similar distribution of CELF members, and re-analysis of single-nucleus RNA sequencing data derived mouse and rat DRG after sciatic injury revealed differential expression of CELFs in specific populations of sensory neurons. We propose that CELF RNA-binding proteins may regulate the fate of mRNAs in populations of nociceptors, and may play a role in pain and/or neuronal regeneration following nerve injury.

INTRODUCTION

RNA binding proteins (RBPs) are critical for orchestrating the post transcriptional fate of transcripts, including transport to sub-cellular domains for local translation, storage and release from ribonucleoprotein complexes and recruitment of translational machinery (e.g., review:

59 (Lenzken et al., 2014)). The 3' untranslated region (3'UTR) of transcripts is a hub for mRNA-
60 protein interactions (e.g., review:(Szostak & Gebauer, 2013)). For example, RBP binding to
61 3'UTRs on nascent transcripts regulates poly(A) signal site selection, cleavage and
62 polyadenylation (e.g., review: (Tian & Manley, 2013). On mature transcripts, 3'UTRs contain
63 interaction sites (originally termed "zip-code" motifs (Kislauskis et al., 1994; Kislauskis & Singer,
64 1992; Ross et al., 1997), for subcellular trafficking (Arora et al., 2022; Kim et al., 2015; Ribeiro
65 et al., 2020; Yergert et al., 2021) anchoring points for scaffolding interactions (Sahoo et al.,
66 2018) and interaction sites for recruitment of miRNAs (Grimson et al., 2007; Majoros & Ohler,
67 2007) or inhibition by competition for binding sites (Srikantan et al., 2012).

68 3'UTR-protein interactions are highly dynamic and provide a regulatory layer for modulation of
69 diverse cellular functions. By interaction with alternative cleavage sites at the distal end of
70 nascent transcripts, RBP-3'UTR interactions generate alternate 3'UTR isoforms through a
71 mechanism termed Alternative Polyadenylation (APA) (Singh et al., 2009). mRNA isoforms with
72 long 3'UTRs are predominantly expressed during development (Ji & Tian, 2009), and in the
73 adult are restricted to certain cell types most notably neurons that express mRNAs with long
74 3'UTRs (Harrison et al., 2014). Differential expression of 3'UTR isoforms by APA is associated
75 with diverse biological functions, for example long 3'UTR isoforms upregulated during
76 neuroplasticity (An et al., 2008; Miura et al., 2013) and during responses to stress (Graber et al.,
77 2013; Zheng et al., 2018), etc. 3'UTR variants are associated with human disease (Griesemer et
78 al., 2021). For example, shortened 3'UTR sequences contain fewer interactions sites for micro-
79 RNAs, and are associated with neurological disease such as Huntington's (Romo et al., 2017),
80 and facilitate oncogene activation and tumor growth (Mayr & Bartel, 2009).

81 RBP-3'UTR interactions are especially important for remote cellular compartments that rely on a
82 supply of mRNA for local protein synthesis. Sensory neurons have extremely long axons
83 projecting from peripheral targets through their cell bodies (soma) housed in DRG terminating in

84 the spinal cord dorsal horn. These termini require a supply of raw materials and machinery that
85 is transported along neuronal processes. RBPs are required for mRNA transport to and
86 translation in these remote domains for maintenance of synapses and for plasticity (Hornberg &
87 Holt, 2013; Wagnon et al., 2012). Numerous “neuron-specific” RBPs have been identified that
88 are highly enriched in neurons and are required for mRNA transport and neuronal excitability
89 (Darnell, 2013; Hornberg & Holt, 2013).

90 Primary somatosensory neurons are classified according to their responsiveness to specific
91 stimuli (light touch, temperature, stretch, etc.), neurochemistry and neurophysiology (Le Pichon
92 & Chesler, 2014), and can be identified by population-specific histological markers. Sensory
93 neurons with unmyelinated axons (C-fibers) tend to have small-diameter cell bodies, and the
94 great majority of these neurons are considered to be nociceptors (reviewed (Light, A.R. 1992)),
95 grossly divided into two subpopulations: peptidergic neurons, which express Calcitonin Gene
96 Related Peptide (CGRP) and Ntrk1 (gene for TRKA) and are particularly important for the
97 transduction of noxious heat stimuli, and non-peptidergic neurons, which bind the plant lectin
98 IB4 and express the G protein-coupled receptor MAS Related GPR Family Member D
99 (MRGPRD) and are particularly important for mechanical nociception (Dong et al., 2001;
100 Silverman & Kruger, 1988). Most sensory neurons that express the heat- and acid-gated
101 channel TRPV1 in adulthood are peptidergic neurons (Zwick et al., 2002). Peptidergic neurons
102 also include a subset of thinly myelinated (A-delta) nociceptors and a minority of A-beta
103 afferents (Lawson et al., 1993, 1996). A third population of C-fibers is comprised of neurons that
104 express tyrosine hydroxylase (TH) and are not nociceptors; instead they are sensitive
105 mechanoreceptors that have been implicated in the transduction of pleasant “social touch”
106 (Lallemend & Ernfors, 2012; Li et al., 2011). Although markers of the peptidergic/non-
107 peptidergic nociceptor populations are highly segregated in the mouse, the selectivity of these
108 markers varies considerably across species; in mouse, IB4-binding is seen in less than 10% of

109 neurons expressing CGRP or TRPV1, whereas in the rat this overlap is 35% (Price & Flores,
110 2007; Zwick et al., 2002), and recent evidence shows that in humans CGRP and TRPV1 are
111 expressed in most nociceptors (IB4 does not bind sensory neurons in human) (Shiers et al.,
112 2021). Recent advances in single-cell RNA-sequencing (scRNA-Seq) allow sensory neurons to
113 be characterized by comprehensive mRNA expression profiles, rather than a handful of
114 neurochemical markers. These transcriptomic studies align closely with histological data and
115 are a powerful resource for identifying the genomic signatures of functionally-distinct neuronal
116 populations (Usoskin et al., 2015).

117 Previously, we reported that functionally distinct populations of DRG neurons express mRNA
118 isoforms with divergent 3'UTR sequences (3'UTR isoforms), and that these 3'UTR variants
119 contain different RBP interaction motifs (Harrison et al., 2019). This led us to theorize that
120 sensory neuron diversity is controlled by differential RBP-3'UTR interactions. In the current
121 study we examine the expression of 3'UTR-binding RBPs in DRG, providing further evidence
122 suggesting divergence of 3'UTR-protein interactions in distinct populations of sensory neurons.

123

124 **METHODS**

125 Animals
126 All animal procedures were approved by the Institutional Animal Care and Use Committee of the
127 University of New England, and Emory University consistent with federal regulations and
128 guidelines. All animals used for this study were 6-8 week old male and female C57/BL6 mice
129 purchased from Jackson Labs (Bar Harbor, Maine).

130 Dorsal Root Ganglion Single Cell RNA-seq Analysis
131 *Trimming, aligning, and quantification*: Previously published single-cell RNA-seq data from adult
132 mouse dorsal root ganglion neurons produced by Usoskin et al. was accessed from GEO using

133 accession code GSE59739 (Usoskin et al., 2015). Fastq files were downloaded and reads were
134 trimmed using Trimmomatic version 0.39 (Bolger et al., 2014) in single-end mode with the
135 following parameters: ILLUMINACLIP:TruSeq3-SE:2:30:10 LEADING:3 TRAILING:3
136 SLIDINGWINDOW:4:15 MINLEN:36. Trimmed reads were aligned to the mouse genome
137 (GRCm38, primary assembly) and transcripts mapping to genes were quantified (Gencode
138 vM25, primary assembly) using STAR version 2.7.5a (Dobin et al., 2013) with default
139 parameters. Transcript quantifications were summed by gene when one cell contained reads
140 from multiple fastq files, and gene counts were tabulated into a gene-by-cell expression matrix.

141 *Clustering, Visualization, and Annotation*: Downstream processing was performed using Seurat
142 version 3.2.0 (Stuart et al., 2019). Cells that expressed fewer than 500 genes, expressed more
143 than 10,000 genes, contained fewer than 1,000 transcripts, or had more than 10% of transcripts
144 mapping to mitochondrial genes were removed, resulting in 811 cells passing all metrics. Gene
145 counts were normalized using “LogNormalize” and counts per 10,000 normalization. 3,000
146 highly variable genes were selected using the “vst” method. Normalized transcript counts were
147 scaled to 0 mean and unit variance, and principal component analysis with 100 principal
148 components was performed. Cells were Louvain clustered with a resolution of 1 and k = 20
149 nearest neighbors resulting in six clusters. Cells were embedded using t-SNE and UMAP with
150 default parameters. A grid search of clustering parameters for k nearest neighbors in {10, 15,
151 20, 30} and resolution in {0.5, 1, 1.5, and 2} was performed with visual inspection of
152 concordance between UMAP embedding and clustering to verify that k = 20 and resolution = 1
153 were reasonable. Normalized gene expression for 12 marker genes (Th, Sst, Mrgprd, P2rx3,
154 Tac1, Ntrk1, Calca, Nefh, Pvalb, B2m, Vim, Col6a2) were plotted and cluster cell types were
155 manually annotated as Non-neuronal, Peptidergic (Pep), non-peptidergic (NP), tyrosine
156 hydroxylase-expressing (TH) and neurofilament heavy chain (Nefh)-expressing (NF) (Fig 1). To
157 identify cell subpopulations, each cell type was separately processed using 2000 variable

158 features, 30 principal components, k = 10 nearest neighbors, and a louvain resolution of 1.

159 *Differential Expression Analysis*: Differentially expressed genes were identified using a Wilcoxon
160 rank sum test for each cell type compared to all other cell types where the log2 fold change was
161 greater than 0.25 and the gene was expressed in at least 10% of cells. A list of all known 3-
162 UTR-binding proteins was obtained from the Gene Ontology consortium website (Ashburner et
163 al., 2000; Gene Ontology Consortium, 2021) to highlight differentially expressed cell type
164 specific 3'UTR-binding proteins.

165 *mRNA co-expression analysis:* Pearson's correlation was calculated by comparison of CELF4
166 mRNA expression values vs expression values for all other detected mRNAs. For reference,
167 also shown are values for CGRP vs NTRK1 (known to be co-expressed in the same population
168 of neurons) and CGRP vs MRGPRD (known to be expressed separately in distinct populations)
169 (Fig 6A).

170 Antibody characterization (Table 1)
171 Polyclonal rabbit anti-CELF4 antibody (Prestige Antibodies, Sigma-Aldrich, HPA037986):
172 Developed using CUGBP, Elav-like family member 4 recombinant protein epitope signature tag
173 (PrEST). This antibody has previously been extensively validated for use with immunostaining:
174 This antibody detected CELF4 protein in the wildtype mouse hippocampal and cortical neurons,
175 but not in the CELF4 knockout samples (Wagnon et al., 2011, 2012). In addition, we determined
176 that CELF4 gene deletion (CELF4-fl/fl (Wagnon et al., 2011) ; Avil-cre-ERT2 mice treated with
177 tamoxifen (Lau et al., 2011) resulted in loss of signals (Fig 4A), as did omission of primary
178 antibody (Fig 6C, 7), providing further evidence that this reagent is specific and robust.

179 Polyclonal guinea pig anti-TRPV1 (Neuromics, GP14100): The antigen was residues of the
180 carboxy-terminus of rat TRPV1, YTGSLKPEDAEVFKDSMVPGEK. This antibody has been
181 assessed with wild-type tissue, as well as TRPV1-deficient mice, and no apparent

182 immunoreactivity was observed in TRPV1-KO mouse DRG, although the antibody robustly
183 stained the expected population of wild-type neurons (Sand et al., 2015). In addition, omission
184 of primary antibody resulted in loss of signals (Fig 6C).

185 Polyclonal chicken anti NF-H (EnCor, CPCA-NF-H): NF-H antibody robustly stained the
186 expected population of medium and large diameter DRG neurons and large caliber axons. No
187 signal was detected in NF-H negative small diameter neurons, small caliber fibers or non-
188 neuronal cells (Fig 5), thus confirming the specificity of this reagent.

189 Polyclonal guinea pig anti-CGRP (20R-CP001): CGRP antibody was raised in guinea pig using
190 calcitonin gene-related peptide conjugated to BSA as the immunogen. This antibody has been
191 extensively used for immunostaining DRG tissue slices to identify peptidergic neurons, and
192 specifically stains this population (Harrison et al., 2014).

193 Immunofluorescence Imaging and Analysis
194 Immunofluorescent staining was used to characterize populations of DRG neurons that express
195 CELF4 using reagents detailed in Table 1: CGRP for peptidergic, TRPV1 for heat responsive
196 nociceptors, and NF-H for myelinated neurons. Additionally, the plant lectin IB4 conjugated to
197 fluorophore was used to stain the non-peptidergic population, e.g.: (Burnstock, 2000)

198 *Sample Collection and Processing:* Animals were exsanguinated under deep pentobarbital
199 anesthesia, before perfusion with cold 4% paraformaldehyde in PBS. DRG were immediately
200 dissected, fixed in 4% paraformaldehyde (PFA) in PBS for 10 minutes before cryoprotection by
201 incubating overnight in 30% sucrose. 15 μm sections were cut using a cryostat, mounted onto
202 adhesion microscope slides, and left to dry, uncovered at room temperature for at least 1 hour.

203 *Immunostaining:* Non-specific binding sites were blocked by incubating sections with 5% donkey
204 serum in 0.4% Triton X-100 PBS for 1 hour, covered. CELF4 antibody was diluted 1:800,

205 TRPV1 1:500, CGRP 1:1000 and/or NF-H 1:40000 in blocking buffer and left on sections
206 overnight (i.e. 18-24 hours) at room temperature. The sections were then washed with 0.4%
207 Triton X-100 PBS; the washing solution was left on for 5 minutes for the first wash, then 10
208 minutes for the following three washes. Secondary antibodies and counterstains were prepared
209 1:200 in blocking buffer, added to sections and for 2 hours at room temperature. Alexa 488-
210 conjugated IB4 was diluted at 1:50. The sections were washed a second time using the same
211 procedure as the first wash. Slides were coverslipped with an antifade mountant and left
212 overnight at room temperature before imaging.

213 *Imaging:* Multichannel fluorescent micrographs of entire longitudinal DRG sections were
214 obtained using a Leica DMi8 epifluorescent inverted microscope with 20X objective and
215 automated field stitching. Image analysis was performed as previously published (Harrison et
216 al., 2014): Two sections per animal containing more than 200 neurons with visible nuclei were
217 selected from four animals. Sections were spaced more than 50 μm apart to ensure that no
218 single neuron could be included in the analysis twice. Using Image J software (Schneider et al.,
219 2012), individual neurons with visible nuclei were then manually circled to generate separate
220 regions of interest (ROIs). Mean fluorescent intensities were recorded along with the cross-
221 sectional area from each ROI. All ROI data from both sections from individual animals were then
222 collated into a single dataset per animal, yielding data from over 400 neurons per animal.
223 Background was estimated as the mean signal intensity of non-expressing neurons. The
224 median staining intensity for each channel was then calculated for each of the four datasets
225 (i.e., the median intensity of each DRG) to allow for normalization of fluorescence intensities to
226 the mean median value (division by central tendency [median] method). First, to observe the
227 distribution of CELF4 expression according to neuron soma size, normalized signals from all
228 animals were collated into a single dataset and subsequently binned according to soma cross-
229 sectional area (50μm bin sizes) (Fig. 4C). Neurons were assigned to either small (<300μm),

230 medium (300-700μm) or large (>700μm) populations. These size divisions were chosen due to
231 the well-established somatosensory characteristics that vary according to soma size. To
232 identify peptidergic, non-peptidergic and myelinated populations, sections were co-stained with
233 CGRP antibody, IB4 lectin or neurofilament heavy chain (NF-H) antibody respectively
234 (Ruscheweyh et al., 2007).

235 *Neuronal Retrograde Tracing:* For retrograde labeling of muscle afferents, 8 adult wild type
236 C57BL/6J mice (Jackson Laboratories, strain #000664) at least 8-weeks of age were studied.
237 The right bilateral heads of the gastrocnemius and tibialis anterior muscles received 2μL
238 injections of 5.0% fast blue retrograde tracer (Polysciences, 17740) with a 26-gauge 10μL
239 Hamilton microliter syringe (Model #701) distributed in at least 3 areas within the muscle
240 bellies under 2% isoflurane (Piramal Enterprises Limited, Telangana, India, ANADA 200-237,
241 NDC 66794-013-25) in 1L/min O_2, totaling 6μL of tracer. All mice received 1 dose of 5mg/kg
242 1.5mg/ml meloxicam (Pivetal, ANADA 200-550, NDC 46066-170-13). Four to 14 days later, to
243 allow for retrograde transport, mice were euthanized and perfused with 0.4% paraformaldehyde
244 as described above. The right L4 dorsal root ganglion (DRG) was dissected and placed in 20%
245 sucrose for cryoprotection prior to being cryosectioned for immunohistochemistry as detailed
246 above.

247 *Skin Imaging:* For analysis of lanceolate endings, 5 additional wild type C57BL/6J mice were
248 used. Following euthanasia and paraformaldehyde perfusion, a quadrangular piece of hairy hind
249 paw skin was dissected, cryoprotected and sectioned transversely at 30 μm. Following
250 immunolabeling with NF-H and CELF4, the skin was imaged on a Nikon A1R with 60x objective,
251 0.5 μm step size.

252 **RESULTS**

253 To identify RBPs expressed in populations of sensory neurons, we obtained publicly available

254 single-cell RNA-Sequencing data generated from adult mouse DRG (GEO GSE59739) (Usoskin
255 et al., 2015). Since release of those data, analysis tools have evolved significantly. In addition,
256 gene annotations, mapping coordinates and transcript variant sequences are under constant
257 revision. We therefore reanalyzed the raw sequencing data using current software (SEURAT
258 3.2.0) and annotations (Gencode vM25). Cells clustered into functionally defined populations as
259 expected (Fig 1): Peptidergic (PEP) that are predominantly nociceptors that express
260 neuropeptides such as CGRP, non-peptidergic (NP) that are predominantly nociceptors that do
261 not express these neuropeptides, tyrosine hydroxylase-expressing (TH) small-diameter sensory
262 neurons implicated in the pleasurable, affective component of touch and neurofilament heavy
263 chain (NF-H)-expressing that are myelinated and respond to low threshold stimuli such as light
264 touch. Within those clusters, neurons grouped into expected sub populations, for example
265 TRPV1-expressing neurons (heat responsive nociceptors) subclustered within the PEP cluster,
266 and parvalbumin-expressing neurons (chiefly proprioceptors) subclustered within the NF
267 (myelinated) cluster (Fig 1) (Usoskin et al., 2015).

268 Gene expression profiles from each population (Pep, NP, TH, NF) were compared by differential
269 gene expression analysis using Wilcoxon rank sum test with SEURAT software. Of
270 approximately 1100 known RBPs annotated in the mouse genome, 100 are assigned the gene
271 ontology (GO) term “mRNA 3’-UTR binding” (Table 2). Of those, 84 3’UTR-binding proteins
272 were detectable in DRG neurons (expression > 1 CFM) and 17 were enriched in at least 1
273 population (Table 2). Therefore, the majority (80%) of 3’UTR-binding proteins detected in DRG
274 neurons were ubiquitously expressed throughout all populations, as exemplified by FXR1 (Fig 2
275 a,b). Interestingly, 4 members of the CUGBP Elav-Like Family (CELF) were differentially
276 expressed: CELFs 2, 3, 4 and 6 (Table 3, Fig 2). CELF2 was enriched in the PEP population,
277 CELF3 in the TH population, CELF4 in the PEP population and CELF6 was enriched in both NP
278 and PEP populations.

279 During these studies, numerous single-cell/nucleus sequencing studies were published and the
280 data made publicly available. We therefore sought to confirm our findings using single nucleus
281 sequencing data from adult mouse DRG (Renthal et al., 2020), and adult macaque (Kupari et
282 al., 2021). We observed that CELF4 is predominantly in peptidergic populations (Fig. 3 a,b)
283 confirming our previous results. Interestingly, we also observed that CELF1 and 2 are
284 expressed in satellite/glial cells in addition to neurons (Figure 3 a).

285 CELF4 had the highest mean expression value of all family members (Figs. 2,3) and the largest
286 differential expression value (28.2 fold) over the mean (Table 3). This family member negatively
287 regulates neuron excitability in excitatory CNS neurons, likely by limiting translation of mRNAs
288 encoding synaptic proteins and ion channels (Wagnon et al., 2011, 2012). However, expression
289 and function of CELF4 in sensory neurons has not been described. RNA concentration does not
290 necessarily correlate with protein concentration, e.g.:(Edfors et al., 2016). Therefore, the
291 expression of CELF4 protein was examined using quantitative immunofluorescence microscopy.
292 By measurement of fluorescent signals from individual somata from 3 animals (approx. 200
293 somata/animal), we observed that 58% of small diameter (<300 μm) and 38% of medium
294 diameter (300-700 μm) DRG neurons were CELF4 positive (Fig 4). Using established
295 histological markers for non-peptidergic (plant lectin IB4), peptidergic (CGRP antiserum) and
296 myelinated (NFH antiserum) neurons, we observed that CELF4 protein distribution mirrors that
297 of CELF4 mRNA. CELF4 was detected in 53% of CGRP+, 34% of IB4-binding and 54% NF-H+
298 neurons (Fig 5). However, CELF4 protein is expressed to significantly lower levels in IB4-
299 binding ($p<0.05$, $n=3$) and NF-H+ ($p<0.01$, $n=3$ mice) neurons.

300 By comparing CELF4 mRNA expression to that of all other mRNAs detected in the scRNA-Seq
301 dataset, we determined that CELF4 expression is most highly correlated with GFRA3, TRPV1
302 and Calca (gene name for CGRP) expression in adult mouse DRG neurons (Fig 6, a).

303 Given the prominent functional role of TRPV1+ afferents in muscle nociception and mechanical
304 hyperalgesia, we chose to further characterize CELF4 protein expression in peripheral targets
305 by taking advantage of the well-known central and peripheral innervation pattern of the sciatic
306 nerve. Lumbar DRGs 3-5 contribute sensory innervation to peripheral targets to the muscles,
307 vasculature, and skin of the leg. We first performed retrograde tracing from the tibialis anterior
308 and gastrocnemius muscles to specifically label the DRG afferents innervating these muscles.
309 In total, we characterized 2,490 (1 DRG each from 8 mice) retrogradely labeled primary sensory
310 neurons for their expression of CELF4 and TRPV1. Many DRG neurons were CELF4+
311 (n=4876), and approximately 30% of them were also retrogradely labeled. We found that 42% of
312 retrogradely labeled afferents also expressed the neuropeptide TRPV1 in L4 DRG, which
313 agrees with previous findings using femoral nerve tracing and L2 DRG (Christianson et al.,
314 2006). The majority of triple labeled (fast blue, CELF4, TRPV1) neurons was small in
315 diameter. By co-staining DRG sections with TRPV1 and CELF4 antisera, we confirmed that the
316 majority CELF4 immunofluorescence signal intensity is correlated with TRPV1 signal intensity
317 (Fig 6b, c). Furthermore, among all TRPV1+ muscle afferents in the L4 DRG, 76% were also
318 CELF4+.
319 Again, using our predicted CELF4 phenotype (primarily peptidergic – GFRA3, CGRP, TRPV1),
320 we investigated CELF4 expression in another peripheral sensory target. Lanceolate endings are
321 innervated by low threshold mechanoreceptors (LTMRs) whose cell bodies reside in the DRG.
322 These specialized sensory termini are multiply innervated by a combination of Aβ-, Aδ-, and C-
323 LTMRs. The specialized combinations of these sensory endings encode distinct sensory
324 properties based on their myelination status and adaptation rates to sustained stimuli with at
325 least 5 physiologically distinct LTMRs in hairy skin (Kuehn et al., 2019). Given that 90% of the
326 body is covered with hair in most mammals, lanceolate endings are an indispensable unit for the
327 perception of mechanosensory stimuli upon the skin. The majority of these lanceolate endings
328 are also innervated by CGRP+ peptidergic nociceptors, which respond rapidly to hair pull and

329 are developmentally dependent on NGF-TRKA signaling (Ghitani et al., 2017; Li & Ginty, 2014).
330 Together with our finding that CELF4 is expressed in the cell bodies of this population, and that
331 CELF4 is transported to neuropil in the CNS (Wagnon et al., 2012), we reasoned that a large
332 proportion of lanceolate sensory endings in hairy skin would also express CELF4. We identified
333 114 lanceolate endings ~equally sampled among 5 mice, and 49.2% expressed CELF4. The
334 pattern of CELF4 labeling suggests that CELF4 is present in both the circumferential and
335 longitudinal endings surrounding the hair follicle (Fig 7), suggesting that CELF4 is present in the
336 CGRP+ endings and/or at least one population of LTRMs

337 Previous work has shown that CELF4 regulates neuron excitability (Wagnon et al., 2011) and
338 that CELF members may play a role in axon growth (Chen et al., 2016). We therefore wanted to
339 examine the expression of CELF proteins in a model of nerve injury where hyperexcitable
340 neurons are regenerating. Re-analysis of data from sciatic crush (Renthal et al., 2020) strongly
341 indicated that CELF RNA-binding proteins are differentially expressed during the time course of
342 recovery from sciatic injury (Fig. 8a). This was confirmed by analysis of bulk RNA-seq data
343 derived from rat sensory ganglia post sciatic injury (Harrison et al., 2019) where CELFs are
344 down-regulated during the course of recovery (Fig. 8 b).

345

346 **DISCUSSION**

347 Our previous work has shown that populations of sensory neurons express different mRNA
348 isoforms with alternate 3'UTRs (Harrison et al., 2014). In the current study, we investigated the
349 expression of 3'UTR-binding proteins in DRG, leading to the discovery that members of the
350 CUGBP-binding ELAV-like family of RBPs are expressed in distinct populations of sensory
351 neurons. By analysis of publicly available scRNA-Seq data, we revealed that CELF2 is
352 expressed in small diameter neurons and non-neuronal cells, CELF4 is restricted to the

353 peptidergic (PEP) population, and CELF6 is present in both peptidergic and non-peptidergic
354 (NP) populations. These neuronal populations predominantly represent different classes of C-
355 fiber nociceptors, and in the case of PEP also a subset of A-delta fibers. Most CGRP-
356 expressing (PEP) C-fibers also express the pro-inflammatory neuropeptide substance P
357 (Juránek & Lembeck, 1997). CGRP and SP are pro-inflammatory peptides that play key roles in
358 neurogenic inflammation; CGRP is a potent vasodilator and substance P induces mast cell
359 degranulation (Lim et al., 2017). In contrast, NP neurons have been reported to suppress mast
360 cell reactivity (Zhang et al., 2021). Notably, several studies have demonstrated that cutaneous
361 IB4-binding neurons transduce mechanical stimuli in the non-noxious range, and optogenetic
362 stimulation of these neurons fails to evoke nocifensive behavior unless they are sensitized by
363 tissue injury, calling into question whether these neurons act as nociceptors in healthy tissue
364 (Warwick et al., 2021). CELF3 is restricted to the TH population of non-peptidergic, innocuous
365 low threshold C-fiber mechanoreceptors, which have been implicated in the pleasurable,
366 affective component of touch (Lallemend & Ernfors, 2012; Li et al., 2011). Immunostaining
367 revealed that the family member with the highest expression, CELF4 is enriched in neurons that
368 express the capsaicin receptor TRPV1 and are therefore responsive to noxious heat. CELF4 is
369 a negative regulator of mRNA translation and neural excitability (Wagnon et al., 2011). We
370 therefore propose that further study of CELF4 could uncover mechanisms that regulate protein
371 synthesis in sensory neurons that convey pain and are important for neurogenic inflammation.

372 Previous studies examining the expression profile and function of CELF members have
373 determined that these proteins are expressed in the central nervous system during development
374 and in the adult (Table 4) (Giudice et al., 2016; Krismer et al., 2020; Samaras et al., 2020;
375 Schmidt et al., 2018). The RNA-binding motifs for all members are similar, with UG repeats
376 (Table 4), suggesting that these proteins have the ability to bind similar transcripts. However,
377 given that expression of CELF members is restricted in a cell-type dependent manner, this

378 could limit functional redundancy between members. Focusing on CELF4, in the CNS this
379 member is expressed primarily in excitatory neurons, including large pyramidal cells of the
380 cerebral cortex and hippocampus, where it tonically limits excitatory neurotransmission
381 (Wagnon et al., 2012). In these neurons, RNA-protein interaction profiling (RIP-Seq) revealed
382 that CELF4 predominantly binds to the 3'UTR of transcripts, and CELF4 knockout reduced
383 mRNA stability (Wagnon et al., 2012), and resulted in increases in expression of sodium
384 channel Na(v)1.6 (Sun et al., 2013). Therefore, CELF4 is a negative regulator of excitability of
385 excitatory CNS neurons most likely though limiting translation in these neurons. In accordance,
386 electrophysiological experiments using brain slices revealed that loss of CELF4 function
387 lowered the action potential (AP) initiation threshold and increased AP gain (Sun et al., 2013).

388 This is the first report characterizing expression of CELF4 in populations of neurons in
389 the peripheral nervous system, and its function in those neurons remains unknown.
390 Extrapolating from studies performed with CNS neurons where CELF4 primarily binds to sites
391 within the 3'UTR of mRNAs, indicated molecular functions of this protein could include alternate
392 polyadenylation thereby coordinating the expression of 3'UTR isoforms. This would be an
393 enticing possibility due to our previous observations of differential 3'UTR isoform expression in
394 DRG neuron populations (Harrison et al., 2014), and mechanisms responsible for cell-type
395 specific expression of 3'UTR variants are currently unknown. However, in the current study we
396 did not detect CELF4 in the nucleus of DRG neurons, making this possibility less likely. Also, in
397 the CNS CELF4 mRNA co-sediments with polysomes purified from neuropil, and CELF4
398 knockout increases the concentration of key excitability proteins in this compartment (Wagnon
399 et al., 2012). Therefore, CELF4 limits local translation in CNS axons. Together with our
400 findings, this suggests that CELF4 could also limit protein expression in populations of sensory
401 neuron termini, and experiments to characterize CELF4 expression in central and peripheral
402 endings are currently underway.

403 CELF4 tonically limits protein translation in and excitability of neurons. Therefore,
404 pharmacological targeting of CELF4-3'UTR interactions could lead to the development of tools
405 to study mechanisms of protein translation in neurons. Targeting CELF4 could have wide-
406 ranging implications for diseases of the nervous system. For example in the CNS, CELF4
407 knockout mice develop a seizure phenotype closely resembling an epilepsy syndrome caused
408 by CELF4 locus (18q12) deletion in humans (Halgren et al., 2012). Therefore, enhancing
409 CELF4 function has been proposed as a strategy to treat epilepsy. We have determined that in
410 the PNS CELF4 is enriched in C/Aδ neurons, a population of neurons critical for the etiology of
411 pathological pain, and that this protein is regulated during the time course of recovery from
412 sciatic injury. Therefore, enhancing CELF4 function in nociceptors could be a novel approach to
413 preventing/alleviating chronic pain.

414

415

416 **FIGURE LEGENDS**

417 **Figure 1: Utilization of publicly available single cell RNA sequencing (scRNA-Seq) data,**
418 **derived from adult mouse sensory neurons, to generate population-specific gene**
419 **expression profiles.**

420 To generate gene expression profiles for specific populations of mouse adult sensory neurons,
421 publicly available scRNA-seq data (GSE59739) were downloaded and processed with the latest
422 release of SEURAT software using up to date gene annotations. Graphs are Uniform Manifold
423 Approximation and Projections (UMAPs) of gene expression profiles. Each data point is a cell in
424 UMAP space. Yellow shading = high expression, Blue shading = low expression. Expression
425 profiles distributed into clusters as expected: **A-D** Peptidergic neurons were identified by

426 CALCA (CGRP) expression (PEP, purple cluster), non-peptidergic by MRGPRD expression
427 (NP, green cluster), tyrosine hydroxylase–expressing neurons (TH, red cluster) and myelinated
428 neurons by neurofilament heavy chain expression (NF, blue cluster). **E** Sub-cluster of TRPV1-
429 expressing nociceptors. **F** Sub-cluster of parvalbumin (PVALB) -expressing proprioceptors.

430

431 **Figure 2: The CELF family of RNA-binding proteins are expressed in distinct populations**
432 **of sensory neurons.**

433 **A** Mean vs variance plot of mRNA expression values for 3'UTR-binding RNA-binding protein
434 genes in adult mouse sensory neurons. X's are individual genes. FXR1 and CELF4 are
435 highlighted for reference. **B** Expression of a representative RBP, FXR1 is broadly expressed in
436 all clusters of DRG neurons. Yellow circles are individual neurons that express FXR1 to high
437 levels, blue circles = cells with low FXR1 expression **C** Heatmap of expression values of 3'UTR-
438 binding RBPs significantly differentially expressed (FDR<0.01, top-10) in distinct populations of
439 sensory neurons. Each line shows expression values in a single cell. Yellow = high expression ,
440 Purple = low expression. **D** Expression of significantly differentially expressed CELF-family
441 RBPs in DRG neuron clusters. Yellow = high expression , blue = low expression. **E** Violin plots
442 showing the distribution of expression values for significantly differentially expressed CELF
443 family proteins. Yellow triangles denote significant enrichment, purple triangles denote
444 significant exclusion. TH = tyrosine hydroxylase–expressing, NP = non-peptidergic, NF =
445 neurofilament heavy chain-expressing and PEP = peptidergic neurons.

446

447 **Figure 3: Re-analysis of publicly available single cell RNA-sequencing datasets confirm**
448 **that CELF4 members are expressed in distinct populations of cells in sensory ganglia of**

449 **adult mouse and macaque.**

450 **A** Expression of CELF member mRNAs in populations of neuronal and non-neuronal adult
451 mouse sensory ganglia cells. Data from GSE154659 (Renthal et al., 2020). CELF1 and 2
452 mRNAs are detected in non-neuronal populations, whereas CELF4 is enriched in peptidergic
453 neurons. **B** In the adult macaque, neuronal expression of CELF members is highly similar to
454 mouse. Data from (Kupari et al., 2021).

455

456 **Figure 4**: **CELF4 protein is expressed in small and medium diameter sensory neurons.**

457 **A** CELF4 gene deletion abolishes CELF4 immunoreactivity, confirming the specificity of the
458 CELF4 antibody. **B** Representative immunofluorescent micrograph of a 14μm DRG section
459 stained with CELF4 antibody. **C** Soma size distribution of CELF4+ neurons. Data are collated
460 from 3 sections, from 3 DRG from 3 replicate animals (approx. 100 soma per section). Somata
461 were categorized according to cross-sectional area - small (<300μm), medium (300-700μm) or
462 large (>700μm). **C i** Proportion of small, medium or large cross-sectional area DRG neurons
463 that express CELF4. **ii** Proportion of CELF4-expressing neurons with small, medium or large
464 cross-sectional areas.

465

466 **Figure 5: CELF4 protein expression in peptidergic (CGRP+), non-peptidergic (IB4-**
467 **binding) and myelinated (NF-H+) neurons.**

468 **A-C** 14μm DRG sections stained with CELF4 antibody, co-stained with established histological
469 markers. Peptidergic neurons were identified with CGRP antibody, non-peptidergic with isolectin
470 IB4 and myelinated with NFH. Scatter plots show distribution of fluorescence intensities of

471 somata collated from DRG from 3 replicate animals, 2 non-overlapping cross sections per
472 animal (approx. 100 soma per section). Dashed lines indicate background signals levels. **D** Pie
473 charts showing the proportion of double positive somata from each of the 3 stains. **E** Mean
474 CELF4 fluorescence values. Stats = ANOVA with post hoc t-tests, n=3 animals, *=p<.05,
475 **=p<.01.

476

477 **Figure 6: CELF4 is co-expressed with the TRPV1 capsaicin receptor in DRG neurons.**

478 **(A)** Pearson's r correlation coefficients were calculated for CELF4 mRNA concentration vs all
479 other transcripts. The 3 most positively and negatively correlated genes are shown. Also shown
480 are reference values for a known co-expressed pair of mRNAs (CGRP vs NTRK1) and a pair of
481 mRNA's know to be expressed in different neurons (CGRP vs MRGPRD). (**B)** 14μm DRG
482 sections were stained with CELF4 and TRPV1 antibody, and fluorescence intensity measured in
483 soma of 2 sections from 3 animals. Representative micrographs are shown. (**C)** To support the
484 mRNA correlations, we identified muscle afferents that co-express TRPV1 and CELF4 protein
485 by using retrograde neuronal tracing from the gastrocnemius and tibialis anterior muscles
486 combined with immunohistochemistry. Data collected from 3 DRG from 8 replicate animals
487 (lumbar level 4). Representative micrographs are shown along with the no primary controls.

488

489 **Figure 7: CELF4 is distributed to the peripheral termini of sensory neurons.**

490 The location of lanceolate endings in mouse hind paw hairy skin sections was identified by NFH
491 immunoreactivity. CELF4 was detected in 49.2% of lanceolate sensory nerve endings in hair
492 follicles within both the longitudinal and circumferential portions of the sensory terminals (arrow
493 heads). Representative micrographs are shown along with no primary control. n=5 animals.

494

495 **Figure 8: CELF transcripts are downregulated in sensory ganglia in rodent models of**

496 **neuropathic pain.**

497 Single nucleus sequencing data GSE154659 (Renthal et al., 2020) from mouse DRG (**A**) and

498 bulk homogenate RNA-Seq from rat DRG (Harrison et al., 2019) (**B**) showed differential

499 expression of CELF members post sciatic injury. * = $q<0.05$, ** = $q<0.01$ where q values are

500 determined by Student's t-tests with Bonferroni multiple testing correction.

501

References

An, J. J., Gharami, K., Liao, G.-Y., Woo, N. H., Lau, A. G., Vanevski, F., Torre, E. R., Jones, K. R., Feng, Y., Lu, B., & Xu, B. (2008). Distinct role of long 3' UTR BDNF mRNA in spine morphology and synaptic plasticity in hippocampal neurons. *Cell*, *134*(1), 175–187. PubMed. https://doi.org/10.1016/j.cell.2008.05.045

Arora, A., Castro-Gutierrez, R., Moffatt, C., Eletto, D., Becker, R., Brown, M., Moor, A. E., Russ, H. A., & Taliaferro, J. M. (2022). High-throughput identification of RNA localization elements in neuronal cells. *Nucleic Acids Research*, *50*(18), 10626–10642. https://doi.org/10.1093/nar/gkac763

Ashburner, M., Ball, C. A., Blake, J. A., Botstein, D., Butler, H., Cherry, J. M., Davis, A. P., Dolinski, K., Dwight, S. S., Eppig, J. T., Harris, M. A., Hill, D. P., Issel-Tarver, L., Kasarskis, A., Lewis, S., Matese, J. C., Richardson, J. E., Ringwald, M., Rubin, G. M., & Sherlock, G. (2000). Gene Ontology: Tool for the unification of biology. *Nature Genetics*, *25*(1), 1. https://doi.org/10.1038/75556

Bolger, A. M., Lohse, M., & Usadel, B. (2014). Trimmomatic: A flexible trimmer for Illumina sequence data. *Bioinformatics*, *30*(15), 2114–2120. https://doi.org/10.1093/bioinformatics/btu170

Burnstock, G. (2000). P2X receptors in sensory neurones. *British Journal of Anaesthesia*, *84*(4), 476–488. https://doi.org/10.1093/oxfordjournals.bja.a013473

Chen, L., Liu, Z., Zhou, B., Wei, C., Zhou, Y., Rosenfeld, M. G., Fu, X.-D., Chisholm, A. D., & Jin, Y. (n.d.). CELF RNA binding proteins promote axon regeneration in C. elegans and mammals through alternative splicing of Syntaxins. *ELife*, *5*, e16072. https://doi.org/10.7554/eLife.16072

Christianson, J. A., McIlwrath, S. L., Koerber, H. R., & Davis, B. M. (2006). Transient receptor potential vanilloid 1-immunopositive neurons in the mouse are more prevalent within colon afferents compared to skin and muscle afferents. *Neuroscience*, *140*(1), 247–257. https://doi.org/10.1016/j.neuroscience.2006.02.015

Darnell, R. B. (2013). RNA Protein Interaction in Neurons. *Annual Review of Neuroscience*, *36*, 243–270. https://doi.org/10.1146/annurev-neuro-062912-114322

Dobin, A., Davis, C. A., Schlesinger, F., Drenkow, J., Zaleski, C., Jha, S., Batut, P., Chaisson, M., & Gingeras, T. R. (2013). STAR: Ultrafast universal RNA-seq aligner. *Bioinformatics*, *29*(1), 15–21. https://doi.org/10.1093/bioinformatics/bts635

Dong, X., Han, S., Zylka, M. J., Simon, M. I., & Anderson, D. J. (2001). A diverse family of GPCRs expressed in specific subsets of nociceptive sensory neurons. *Cell*, *106*(5), 619–632. https://doi.org/10.1016/s0092-8674(01)00483-4

Edfors, F., Danielsson, F., Hallström, B. M., Käll, L., Lundberg, E., Pontén, F., Forsström, B., & Uhlén, M. (2016). Gene-specific correlation of RNA and protein levels in human cells and tissues. *Molecular Systems Biology*, *12*(10). https://doi.org/10.15252/msb.20167144

Gene Ontology Consortium. (2021). The Gene Ontology resource: Enriching a GOld mine. *Nucleic Acids Research*, *49*(D1), D325–D334. https://doi.org/10.1093/nar/gkaa1113

Gentleman, R. C., Carey, V. J., Bates, D. M., Bolstad, B., Dettling, M., Dudoit, S., Ellis, B., Gautier, L., Ge, Y., Gentry, J., Hornik, K., Hothorn, T., Huber, W., Iacus, S., Irizarry, R., Leisch, F., Li, C., Maechler, M., Rossini, A. J., … Zhang, J. (2004). Bioconductor: Open software development for computational biology and bioinformatics. *Genome Biology*, *5*(10), R80. https://doi.org/10.1186/gb-2004-5-10-r80

Ghitani, N., Barik, A., Szczot, M., Thompson, J. H., Li, C., Le Pichon, C. E., Krashes, M. J., & Chesler, A. T. (2017). Specialized Mechanosensory Nociceptors Mediating Rapid Responses to Hair Pull. *Neuron*, *95*(4), 944-954.e4. https://doi.org/10.1016/j.neuron.2017.07.024

Giudice, G., Sánchez-Cabo, F., Torroja, C., & Lara-Pezzi, E. (2016). ATtRACT-a database of RNA-binding proteins and associated motifs. *Database: The Journal of Biological Databases and Curation*, *2016*, baw035. https://doi.org/10.1093/database/baw035

Graber, J. H., Nazeer, F. I., Yeh, P., Kuehner, J. N., Borikar, S., Hoskinson, D., & Moore, C. L. (2013). DNA damage induces targeted, genome-wide variation of poly(A) sites in budding yeast. *Genome Research*, *23*(10), 1690–1703. https://doi.org/10.1101/gr.144964.112

Griesemer, D., Xue, J. R., Reilly, S. K., Ulirsch, J. C., Kukreja, K., Davis, J. R., Kanai, M., Yang, D. K., Butts, J. C., Guney, M. H., Luban, J., Montgomery, S. B., Finucane, H. K., Novina, C. D., Tewhey, R., & Sabeti, P. C. (2021). Genome-wide functional screen of 3′UTR variants uncovers causal variants for human disease and evolution. *Cell*, *184*(20), 5247-5260.e19. https://doi.org/10.1016/j.cell.2021.08.025

Grimson, A., Farh, K. K.-H., Johnston, W. K., Garrett-Engele, P., Lim, L. P., & Bartel, D. P. (2007). MicroRNA targeting specificity in mammals: Determinants beyond seed pairing. *Molecular Cell*, *27*(1), 91–105. https://doi.org/10.1016/j.molcel.2007.06.017

Halgren, C., Bache, I., Bak, M., Myatt, M. W., Anderson, C. M., Brøndum-Nielsen, K., & Tommerup, N. (2012). Haploinsufficiency of CELF4 at 18q12.2 is associated with developmental and behavioral disorders, seizures, eye manifestations, and obesity. *European Journal of Human Genetics*, *20*(12), 12. https://doi.org/10.1038/ejhg.2012.92

Harrison, B. J., Flight, R. M., Gomes, C., Venkat, G., Ellis, S. R., Sankar, U., Twiss, J. L., Rouchka, E. C., & Petruska, J. C. (2014). IB4-binding sensory neurons in the adult rat express a novel 3′ UTR-extended isoform of CaMK4 that is associated with its localization to axons. *Journal of Comparative Neurology*, *522*(2), 308–336. https://doi.org/10.1002/cne.23398

Harrison, B. J., Park, J. W., Gomes, C., Petruska, J. C., Sapio, M. R., Iadarola, M. J., Chariker, J. H., & Rouchka, E. C. (2019). Detection of Differentially Expressed Cleavage Site Intervals Within 3’ Untranslated Regions Using CSI-UTR Reveals Regulated Interaction Motifs. *Frontiers in Genetics*, *10*, 182. https://doi.org/10.3389/fgene.2019.00182

Hornberg, H. K., & Holt, C. (2013). RNA-binding proteins and translational regulation in axons and growth cones. *Frontiers in Neuroscience*, *7*. https://doi.org/10.3389/fnins.2013.00081

Huber, W., Carey, V. J., Gentleman, R., Anders, S., Carlson, M., Carvalho, B. S., Bravo, H. C., Davis, S., Gatto, L., Girke, T., Gottardo, R., Hahne, F., Hansen, K. D., Irizarry, R. A., Lawrence, M., Love, M. I., MacDonald, J., Obenchain, V., Oleś, A. K., … Morgan, M. (2015). Orchestrating high-throughput genomic analysis with Bioconductor. *Nature Methods*, *12*(2), 115–121. https://doi.org/10.1038/nmeth.3252

Ji, Z., & Tian, B. (2009). Reprogramming of 3′ Untranslated Regions of mRNAs by Alternative Polyadenylation in Generation of Pluripotent Stem Cells from Different Cell Types. *PLoS ONE*, *4*(12). https://doi.org/10.1371/journal.pone.0008419

Juránek, I., & Lembeck, F. (1997). Afferent C-fibres release substance P and glutamate. *Canadian Journal of Physiology and Pharmacology*, *75*(6), 661–664.

Kim, H. H., Lee, S. J., Gardiner, A. S., Perrone-Bizzozero, N. I., & Yoo, S. (2015). Different motif requirements for the localization zipcode element of β-actin mRNA binding by HuD and ZBP1. *Nucleic Acids Research*, *43*(15), 7432–7446. https://doi.org/10.1093/nar/gkv699

Kislauskis, E. H., & Singer, R. H. (1992). Determinants of mRNA localization. *Current Opinion in Cell Biology*, *4*(6), 975–978. https://doi.org/10.1016/0955-0674(92)90128-y

Kislauskis, E. H., Zhu, X., & Singer, R. H. (1994). Sequences responsible for intracellular localization of beta-actin messenger RNA also affect cell phenotype. *The Journal of Cell Biology*, *127*(2), 441–451. https://doi.org/10.1083/jcb.127.2.441

Krismer, K., Bird, M. A., Varmeh, S., Handly, E. D., Gattinger, A., Bernwinkler, T., Anderson, D. A., Heinzel, A., Joughin, B. A., Kong, Y. W., Cannell, I. G., & Yaffe, M. B. (2020a). Transite: A Computational Motif-Based Analysis Platform That Identifies RNA-Binding Proteins Modulating Changes in Gene Expression. *Cell Reports*, *32*(8). https://doi.org/10.1016/j.celrep.2020.108064

Krismer, K., Bird, M. A., Varmeh, S., Handly, E. D., Gattinger, A., Bernwinkler, T., Anderson, D. A., Heinzel, A., Joughin, B. A., Kong, Y. W., Cannell, I. G., & Yaffe, M. B. (2020b). Transite: A Computational Motif-Based Analysis Platform That Identifies RNA-Binding Proteins Modulating

Changes in Gene Expression. *Cell Reports*, *32*(8), 108064. https://doi.org/10.1016/j.celrep.2020.108064

Kuehn, E. D., Meltzer, S., Abraira, V. E., Ho, C.-Y., & Ginty, D. D. (2019). Tiling and somatotopic alignment of mammalian low-threshold mechanoreceptors. *Proceedings of the National Academy of Sciences of the United States of America*, *116*(19), 9168–9177. https://doi.org/10.1073/pnas.1901378116

Kupari, J., Usoskin, D., Parisien, M., Lou, D., Hu, Y., Fatt, M., Lönnerberg, P., Spångberg, M., Eriksson, B., Barkas, N., Kharchenko, P. V., Loré, K., Khoury, S., Diatchenko, L., & Ernfors, P. (2021). Single cell transcriptomics of primate sensory neurons identifies cell types associated with chronic pain. *Nature Communications*, *12*(1), 1510. https://doi.org/10.1038/s41467-021-21725-z

Lallemend, F., & Ernfors, P. (2012). Molecular interactions underlying the specification of sensory neurons. *Trends in Neurosciences*, *35*(6), 373–381. https://doi.org/10.1016/j.tins.2012.03.006

Lau, J., Minett, M. S., Zhao, J., Dennehy, U., Wang, F., Wood, J. N., & Bogdanov, Y. D. (2011). Temporal control of gene deletion in sensory ganglia using a tamoxifen-inducible Advillin-Cre-ERT2 recombinase mouse. *Molecular Pain*, *7*, 100. https://doi.org/10.1186/1744-8069-7-100

Lawson, S. N., McCarthy, P. W., & Prabhakar, E. (1996). Electrophysiological properties of neurones with CGRP-like immunoreactivity in rat dorsal root ganglia. *The Journal of Comparative Neurology*, *365*(3), 355–366. https://doi.org/10.1002/(SICI)1096-9861(19960212)365:3<355::AID-CNE2>3.0.CO;2-3

Lawson, S. N., Perry, M. J., Prabhakar, E., & McCarthy, P. W. (1993). Primary sensory neurones: Neurofilament, neuropeptides, and conduction velocity. *Brain Research Bulletin*, *30*(3–4), 239–243. https://doi.org/10.1016/0361-9230(93)90250-f

Le Pichon, C. E., & Chesler, A. T. (2014). The functional and anatomical dissection of somatosensory subpopulations using mouse genetics. *Frontiers in Neuroanatomy*, *8*, 21–21. PubMed. https://doi.org/10.3389/fnana.2014.00021

Lenzken, S. C., Achsel, T., Carrì, M. T., & Barabino, S. M. L. (2014). Neuronal RNA-binding proteins in health and disease. *Wiley Interdisciplinary Reviews. RNA*, *5*(4), 565–576. https://doi.org/10.1002/wrna.1231

Li, L., & Ginty, D. D. (2014). The structure and organization of lanceolate mechanosensory complexes at mouse hair follicles. *ELife*, *3*, e01901. https://doi.org/10.7554/eLife.01901

Li, L., Rutlin, M., Abraira, V. E., Cassidy, C., Kus, L., Gong, S., Jankowski, M. P., Luo, W., Heintz, N., Koerber, H. R., Woodbury, C. J., & Ginty, D. D. (2011). The functional organization of cutaneous low-threshold mechanosensory neurons. *Cell*, *147*(7), 1615–1627. https://doi.org/10.1016/j.cell.2011.11.027

Light, A. R. (n.d.). *The Initial Processing of Pain and Its Descending Control: Spinal and Trigeminal Systems | Karger Book*. Retrieved February 1, 2023, from https://www.karger.com/Book/Home/222289

Lim, J. E., Chung, E., & Son, Y. (2017). A neuropeptide, Substance-P, directly induces tissue-repairing M2 like macrophages by activating the PI3K/Akt/mTOR pathway even in the presence of IFNγ. *Scientific Reports*, *7*(1), 9417. https://doi.org/10.1038/s41598-017-09639-7

Majoros, W. H., & Ohler, U. (2007). Spatial preferences of microRNA targets in 3’ untranslated regions. *BMC Genomics*, *8*(1), 152. https://doi.org/10.1186/1471-2164-8-152

Mayr, C., & Bartel, D. P. (2009). Widespread Shortening of 3′UTRs by Alternative Cleavage and Polyadenylation Activates Oncogenes in Cancer Cells. *Cell*, *138*(4), 673–684. https://doi.org/10.1016/j.cell.2009.06.016

Mi, H., Ebert, D., Muruganujan, A., Mills, C., Albou, L.-P., Mushayamaha, T., & Thomas, P. D. (2021). PANTHER version 16: A revised family classification, tree-based classification tool, enhancer regions and extensive API. *Nucleic Acids Research*, *49*(D1), D394–D403. https://doi.org/10.1093/nar/gkaa1106

Miura, P., Shenker, S., Andreu-Agullo, C., Westholm, J. O., & Lai, E. C. (2013). Widespread and extensive lengthening of 3' UTRs in the mammalian brain. *Genome Research*, *23*(5), 812–825. https://doi.org/10.1101/gr.146886.112

Price, T. J., & Flores, C. M. (2007). Critical evaluation of the colocalization between calcitonin gene-related peptide, substance P, transient receptor potential vanilloid subfamily type 1 immunoreactivities, and isolectin B4 binding in primary afferent neurons of the rat and mouse. *The Journal of Pain: Official Journal of the American Pain Society*, *8*(3), 263–272. https://doi.org/10.1016/j.jpain.2006.09.005

Renthal, W., Tochitsky, I., Yang, L., Cheng, Y.-C., Li, E., Kawaguchi, R., Geschwind, D. H., & Woolf, C. J. (2020). Transcriptional Reprogramming of Distinct Peripheral Sensory Neuron Subtypes after Axonal Injury. *Neuron*, *108*(1), 128-144.e9. https://doi.org/10.1016/j.neuron.2020.07.026

Ribeiro, D. M., Prod'homme, A., Teixeira, A., Zanzoni, A., & Brun, C. (2020). The role of 3'UTR-protein complexes in the regulation of protein multifunctionality and subcellular localization. *Nucleic Acids Research*, *48*(12), 6491–6502. https://doi.org/10.1093/nar/gkaa462

Romo, L., Ashar-Patel, A., Pfister, E., & Aronin, N. (2017). Alterations in mRNA 3′ UTR Isoform Abundance Accompany Gene Expression Changes in Human Huntington's Disease Brains. *Cell Reports*, *20*(13), 3057–3070. https://doi.org/10.1016/j.celrep.2017.09.009

Ross, A. F., Oleynikov, Y., Kislauskis, E. H., Taneja, K. L., & Singer, R. H. (1997). Characterization of a beta-actin mRNA zipcode-binding protein. *Molecular and Cellular Biology*, *17*(4), 2158–2165.

Ruscheweyh, R., Forsthuber, L., Schoffnegger, D., & Sandkühler, J. (2007). Modification of classical neurochemical markers in identified primary afferent neurons with Aβ-, Aδ-, and C-fibers after chronic constriction injury in mice. *Journal of Comparative Neurology*, *502*(2), 325–336. https://doi.org/10.1002/cne.21311

Sahoo, P. K., Lee, S. J., Jaiswal, P. B., Alber, S., Kar, A. N., Miller-Randolph, S., Taylor, E. E., Smith, T., Singh, B., Ho, T. S.-Y., Urisman, A., Chand, S., Pena, E. A., Burlingame, A. L., Woolf, C. J., Fainzilber, M., English, A. W., & Twiss, J. L. (2018). Axonal G3BP1 stress granule protein limits

axonal mRNA translation and nerve regeneration. *Nature Communications*, *9*(1), 3358. https://doi.org/10.1038/s41467-018-05647-x

Samaras, P., Schmidt, T., Frejno, M., Gessulat, S., Reinecke, M., Jarzab, A., Zecha, J., Mergner, J., Giansanti, P., Ehrlich, H.-C., Aiche, S., Rank, J., Kienegger, H., Krcmar, H., Kuster, B., & Wilhelm, M. (2020). ProteomicsDB: A multi-omics and multi-organism resource for life science research. *Nucleic Acids Research*, *48*(D1), D1153–D1163. https://doi.org/10.1093/nar/gkz974

Sand, C. A., Grant, A. D., & Nandi, M. (2015). Vascular Expression of Transient Receptor Potential Vanilloid 1 (TRPV1). *Journal of Histochemistry and Cytochemistry*, *63*(6), 449–453. https://doi.org/10.1369/0022155415581014

Schmidt, T., Samaras, P., Frejno, M., Gessulat, S., Barnert, M., Kienegger, H., Krcmar, H., Schlegl, J., Ehrlich, H.-C., Aiche, S., Kuster, B., & Wilhelm, M. (2018). ProteomicsDB. *Nucleic Acids Research*, *46*(D1), D1271–D1281. https://doi.org/10.1093/nar/gkx1029

Schneider, C. A., Rasband, W. S., & Eliceiri, K. W. (2012). NIH Image to ImageJ: 25 years of image analysis. *Nature Methods*, *9*(7), 7. https://doi.org/10.1038/nmeth.2089

Shiers, S. I., Sankaranarayanan, I., Jeevakumar, V., Cervantes, A., Reese, J. C., & Price, T. J. (2021). Convergence of peptidergic and non-peptidergic protein markers in the human dorsal root ganglion and spinal dorsal horn. *The Journal of Comparative Neurology*, *529*(10), 2771–2788. https://doi.org/10.1002/cne.25122

Silverman, J. D., & Kruger, L. (1988). Lectin and neuropeptide labeling of separate populations of dorsal root ganglion neurons and associated “nociceptor” thin axons in rat testis and cornea whole-mount preparations. *Somatosensory Research*, *5*(3), 259–267. https://doi.org/10.3109/07367228809144630

Singh, P., Alley, T. L., Wright, S. M., Kamdar, S., Schott, W., Wilpan, R. Y., Mills, K. D., & Graber, J. H. (2009). Global changes in processing of mRNA 3’ untranslated regions characterize clinically distinct cancer subtypes. *Cancer Research*, *69*(24), 9422–9430. https://doi.org/10.1158/0008-5472.CAN-09-2236

Srikantan, S., Tominaga, K., & Gorospe, M. (2012). Functional interplay between RNA-binding protein HuR and microRNAs. *Current Protein & Peptide Science*, *13*(4), 372–379.

Stuart, T., Butler, A., Hoffman, P., Hafemeister, C., Papalexi, E., Mauck, W. M., Hao, Y., Stoeckius, M., Smibert, P., & Satija, R. (2019). Comprehensive Integration of Single-Cell Data. *Cell*, *177*(7), 1888-1902.e21. https://doi.org/10.1016/j.cell.2019.05.031

Sun, W., Wagnon, J. L., Mahaffey, C. L., Briese, M., Ule, J., & Frankel, W. N. (2013). Aberrant sodium channel activity in the complex seizure disorder of Celf4 mutant mice. *The Journal of Physiology*, *591*(1), 241–255. https://doi.org/10.1113/jphysiol.2012.240168

Szostak, E., & Gebauer, F. (2013). Translational control by 3′-UTR-binding proteins. *Briefings in Functional Genomics*, *12*(1), 58–65. https://doi.org/10.1093/bfgp/els056

Tian, B., & Manley, J. L. (2013). Alternative cleavage and polyadenylation: The long and short of it. *Trends in Biochemical Sciences*, *38*(6), 312–320. https://doi.org/10.1016/j.tibs.2013.03.005

Usoskin, D., Furlan, A., Islam, S., Abdo, H., Lönnerberg, P., Lou, D., Hjerling-Leffler, J., Haeggström, J., Kharchenko, O., Kharchenko, P. V., Linnarsson, S., & Ernfors, P. (2015a). Unbiased classification of sensory neuron types by large-scale single-cell RNA sequencing. *Nature Neuroscience*, *18*(1), 145–153. https://doi.org/10.1038/nn.3881

Usoskin, D., Furlan, A., Islam, S., Abdo, H., Lönnerberg, P., Lou, D., Hjerling-Leffler, J., Haeggström, J., Kharchenko, O., Kharchenko, P. V., Linnarsson, S., & Ernfors, P. (2015b). Unbiased classification of sensory neuron types by large-scale single-cell RNA sequencing. *Nature Neuroscience*, *18*(1), 145–153. https://doi.org/10.1038/nn.3881

Wagnon, J. L., Briese, M., Sun, W., Mahaffey, C. L., Curk, T., Rot, G., Ule, J., & Frankel, W. N. (2012). CELF4 Regulates Translation and Local Abundance of a Vast Set of mRNAs, Including Genes Associated with Regulation of Synaptic Function. *PLoS Genetics*, *8*(11). https://doi.org/10.1371/journal.pgen.1003067

Wagnon, J. L., Mahaffey, C. L., Sun, W., Yang, Y., Chao, H.-T., & Frankel, W. N. (2011). Etiology of a genetically complex seizure disorder in Celf4 mutant mice. *Genes, Brain, and Behavior*, *10*(7), 765–777. https://doi.org/10.1111/j.1601-183X.2011.00717.x

Warwick, C., Cassidy, C., Hachisuka, J., Wright, M. C., Baumbauer, K. M., Adelman, P. C., Lee, K. H., Smith, K. M., Sheahan, T. D., Ross, S. E., & Koerber, H. R. (2021). MrgprdCre lineage neurons mediate optogenetic allodynia through an emergent polysynaptic circuit. *Pain*, *162*(7), 2120–2131. https://doi.org/10.1097/j.pain.0000000000002227

Yergert, K. M., Doll, C. A., O'Rouke, R., Hines, J. H., & Appel, B. (2021). Identification of 3' UTR motifs required for mRNA localization to myelin sheaths in vivo. *PLoS Biology*, *19*(1), e3001053. https://doi.org/10.1371/journal.pbio.3001053

Zhang, S., Edwards, T. N., Chaudhri, V. K., Wu, J., Cohen, J. A., Hirai, T., Rittenhouse, N., Schmitz, E. G., Zhou, P. Y., McNeil, B. D., Yang, Y., Koerber, H. R., Sumpter, T. L., Poholek, A. C., Davis, B. M., Albers, K. M., Singh, H., & Kaplan, D. H. (2021). Nonpeptidergic neurons suppress mast cells via glutamate to maintain skin homeostasis. *Cell*, *184*(8), 2151-2166.e16. https://doi.org/10.1016/j.cell.2021.03.002

Zheng, D., Wang, R., Ding, Q., Wang, T., Xie, B., Wei, L., Zhong, Z., & Tian, B. (2018). Cellular stress alters 3'UTR landscape through alternative polyadenylation and isoform-specific degradation. *Nature Communications*, *9*(1), 2268. https://doi.org/10.1038/s41467-018-04730-7

Zwick, M., Davis, B. M., Woodbury, C. J., Burkett, J. N., Koerber, H. R., Simpson, J. F., & Albers, K. M. (2002). Glial cell line-derived neurotrophic factor is a survival factor for isolectin B4-positive, but not vanilloid receptor 1-positive, neurons in the mouse. *The Journal of Neuroscience: The Official Journal of the Society for Neuroscience*, *22*(10), 4057–4065. https://doi.org/20026394

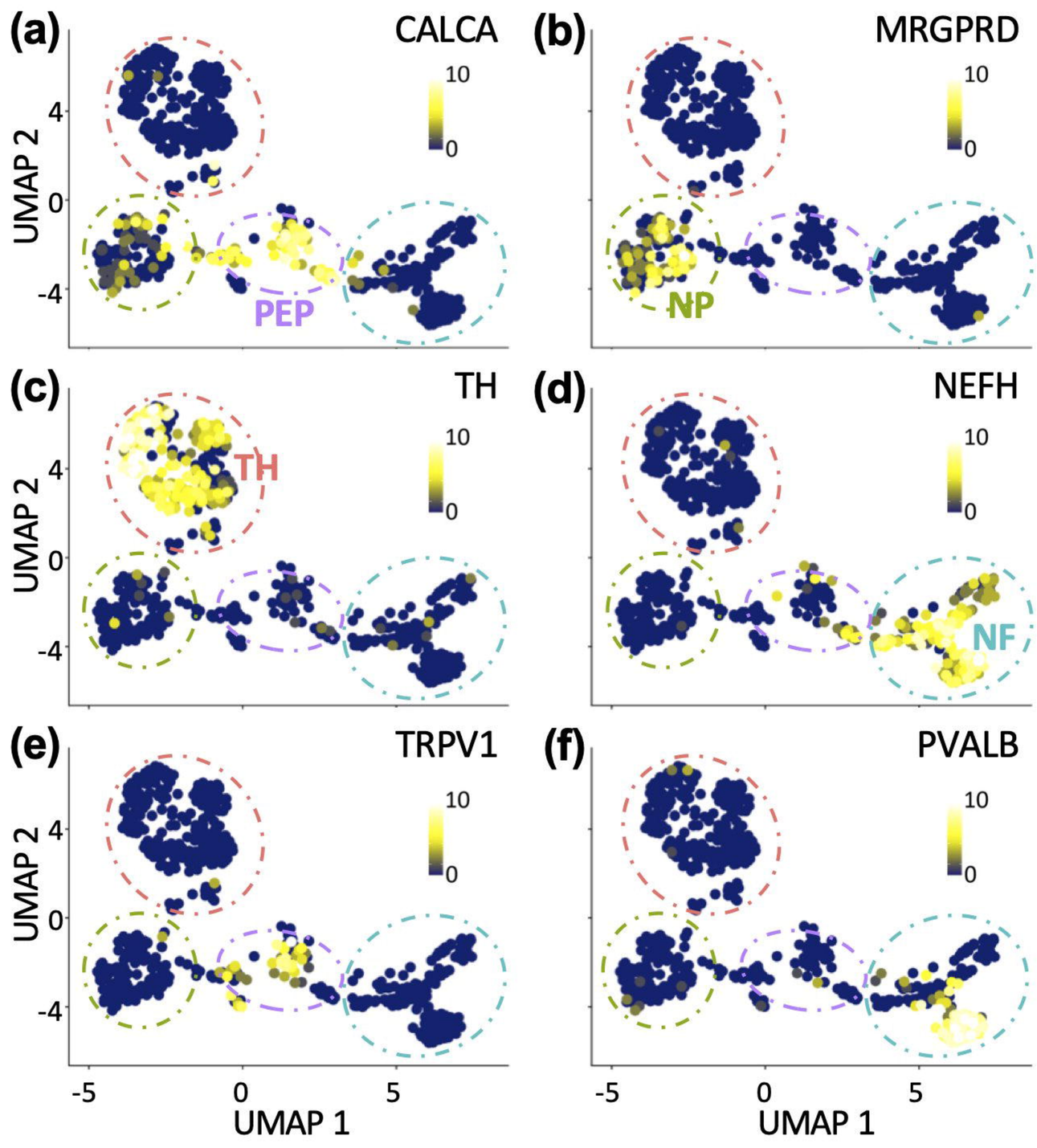

Figure 1 (Methods)

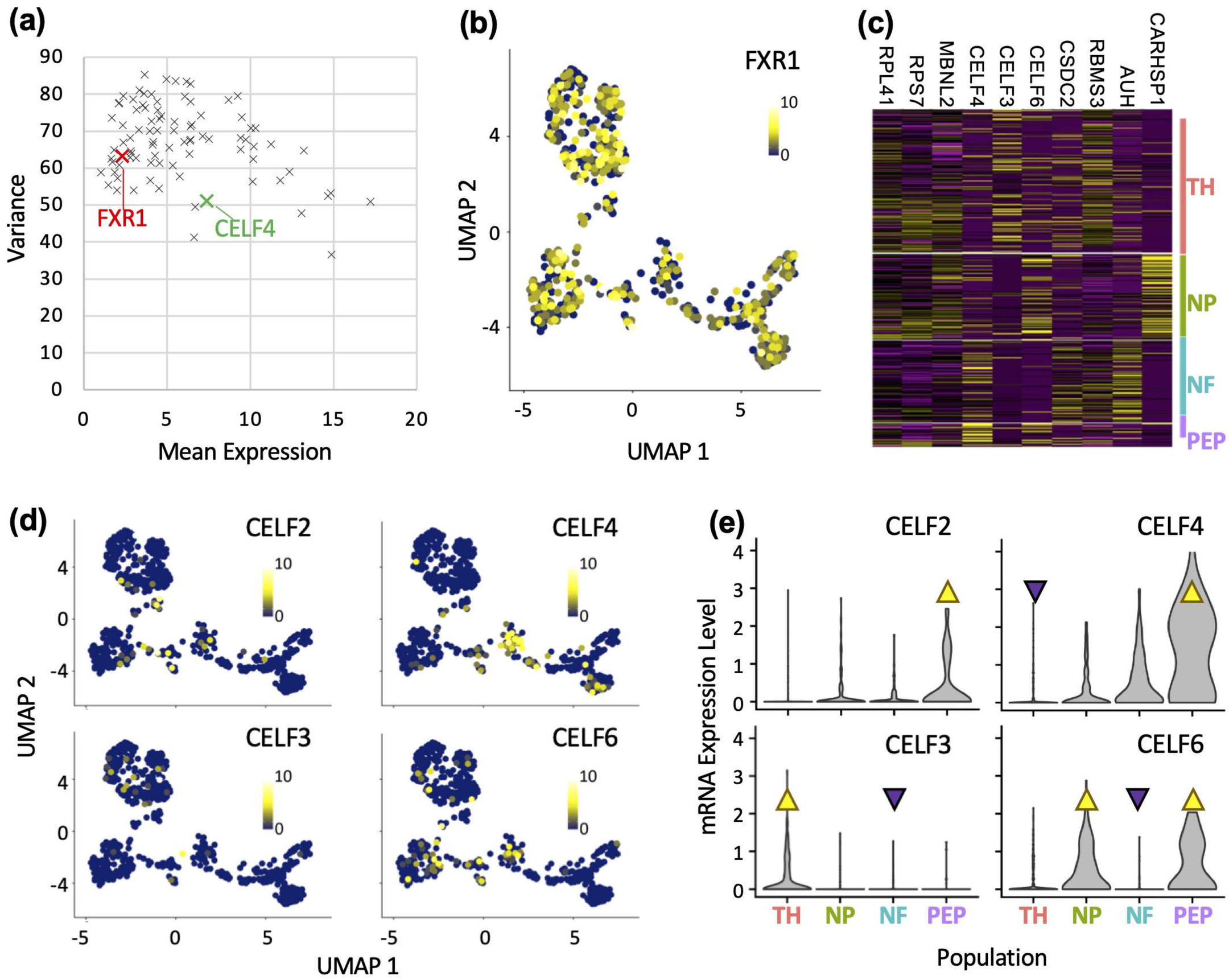
(a)
Variance
Mean Expression
FXR1
CELF4
(b)
FXR1
UMAP 2
UMAP 1
(c)
RPL41
RPS7
MBNL2
CELF4
CELF3
CELF6
CSDC2
RBMS3
AUH
CARHSP1
TH
NP
NF
PEP
(d)
CELF2
CELF4
CELF3
CELF6
UMAP 2
UMAP 1
(e)
CELF2
CELF4
CELF3
CELF6
mRNA Expression Level
TH
NP
NF
PEP
Population

Figure 2

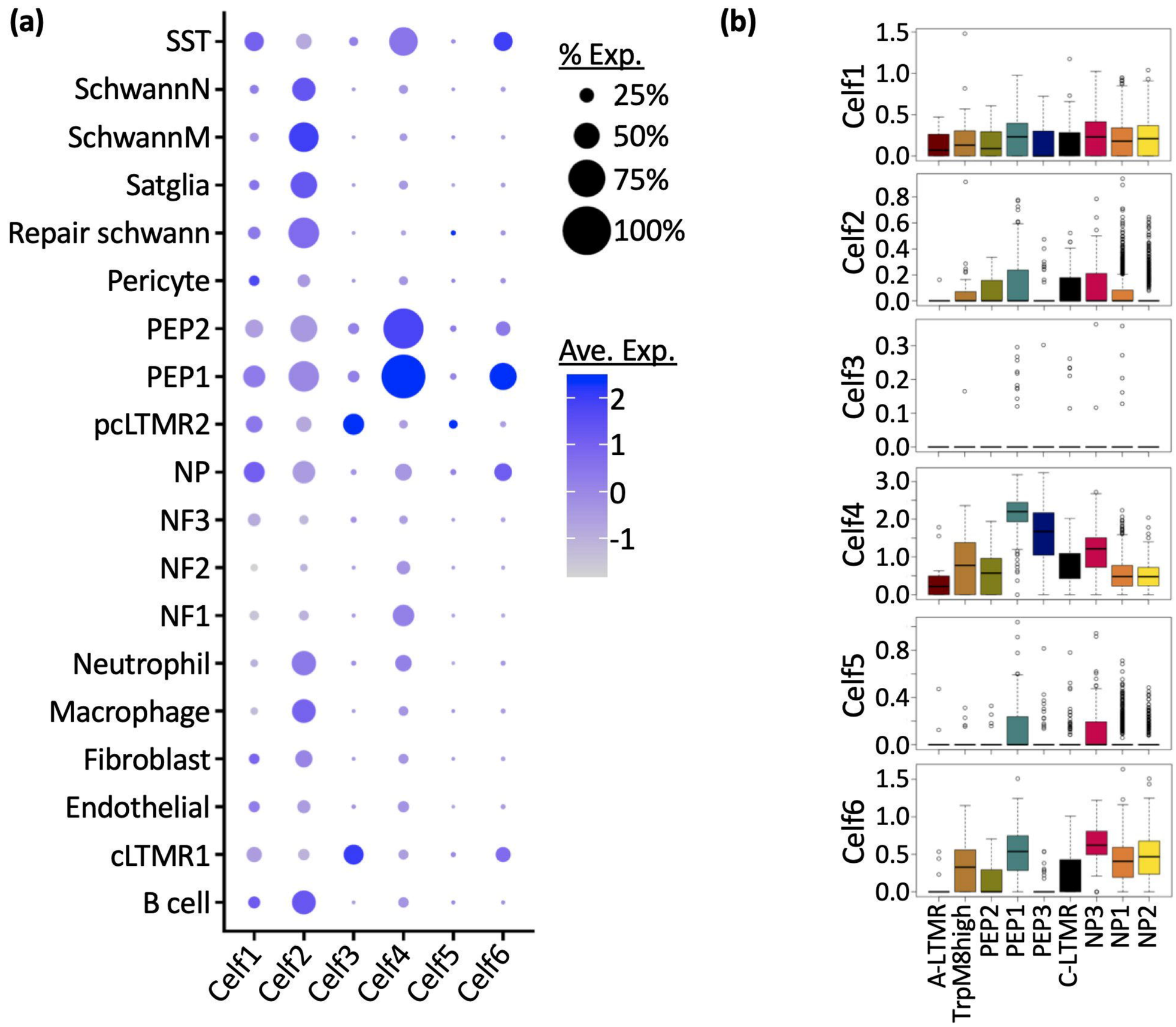
(a)
SST
SchwannN
SchwannM
Satglia
Repair schwann
Pericyte
PEP2
PEP1
pcLTMR2
NP
NF3
NF2
NF1
Neutrophil
Macrophage
Fibroblast
Endothelial
cLTMR1
B cell
Celf1
Celf2
Celf3
Celf4
Celf5
Celf6
% Exp.
25%
50%
75%
100%
Ave. Exp.
2
1
0
-1
(b)
Celf1
Celf2
Celf3
Celf4
Celf5
Celf6
A-LTMR
TrpM8high
PEP2
PEP1
PEP3
C-LTMR
NP3
NP1
NP2

Figure 3

(a)

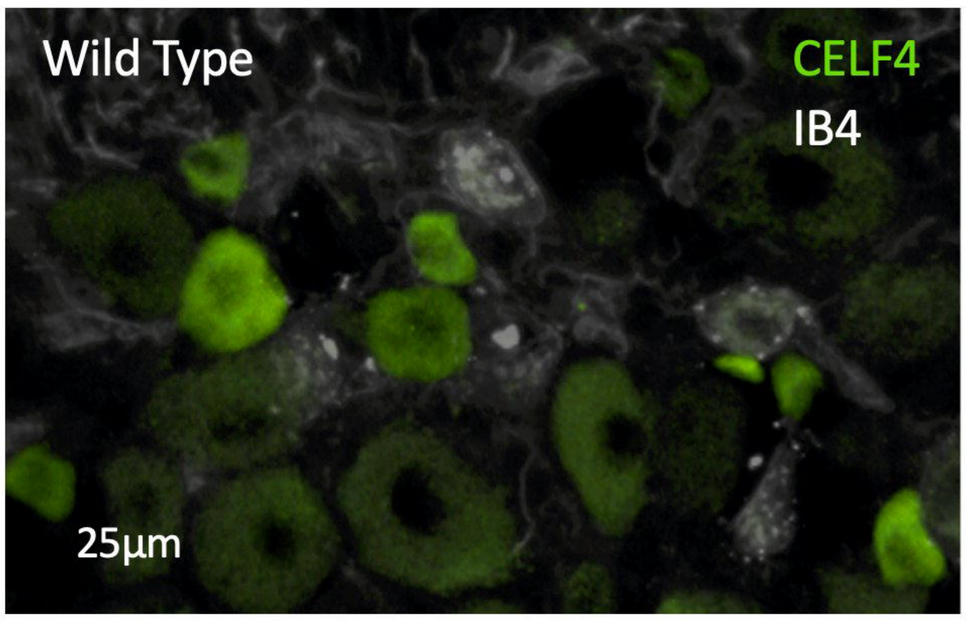

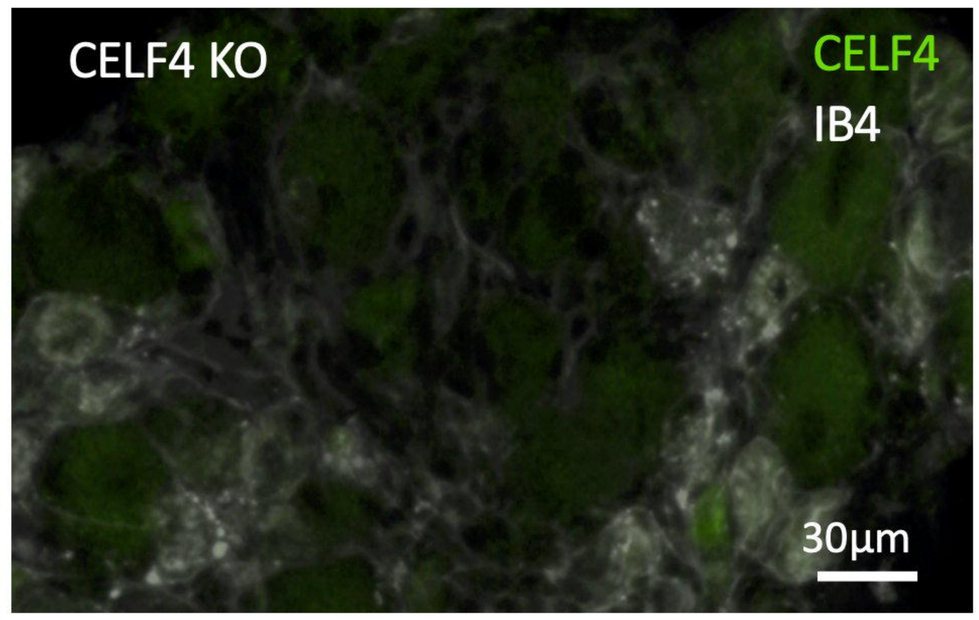

(b)

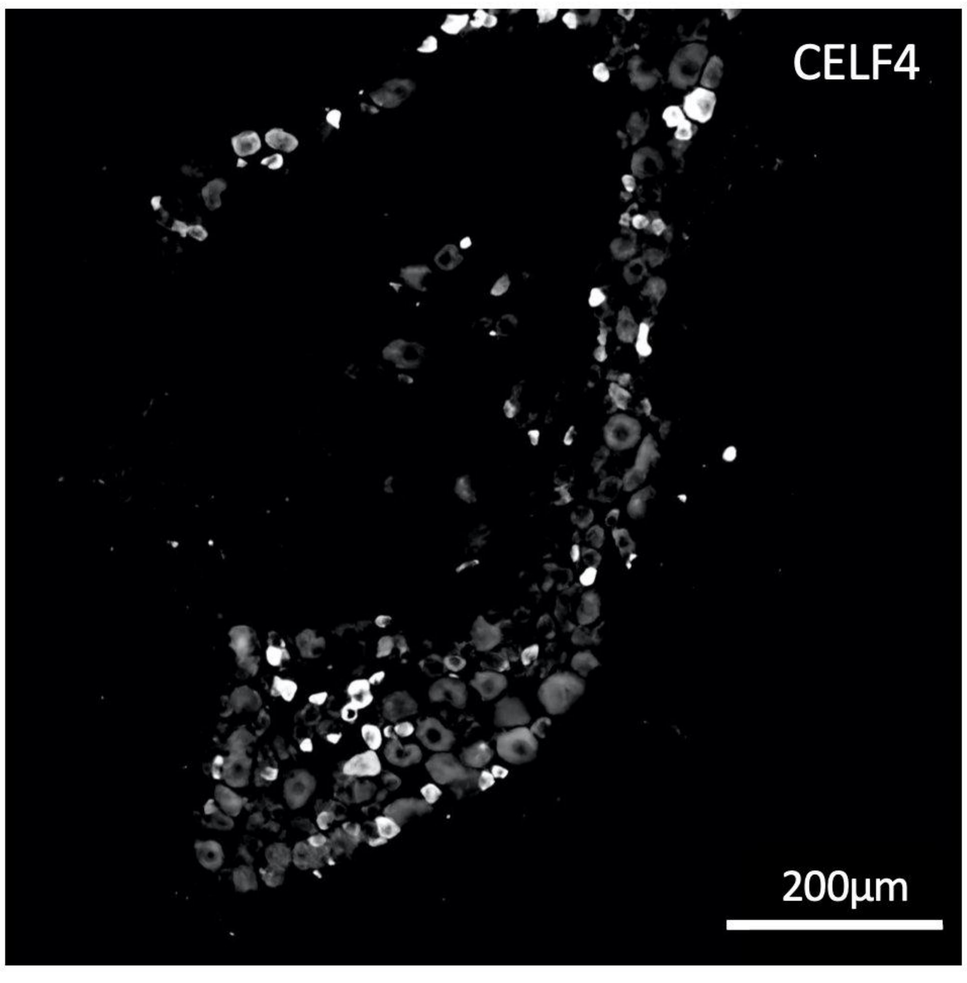

(c)

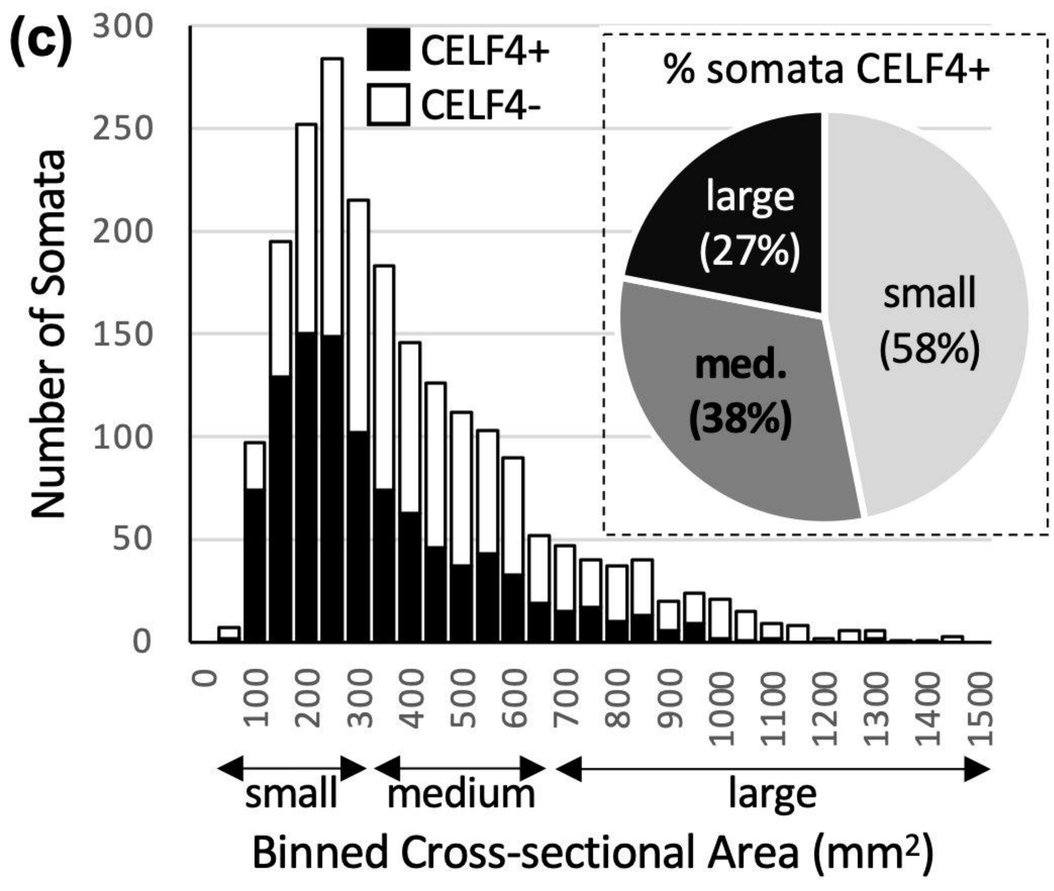

	(i) % somata CELF4+	(ii) % CELF4+ somata
Small (<300)	57.7	60.7
Medium (300-700)	38.4	33.0
Large (>700)	27.0	6.3
All	46.6	n/a

Figure 4

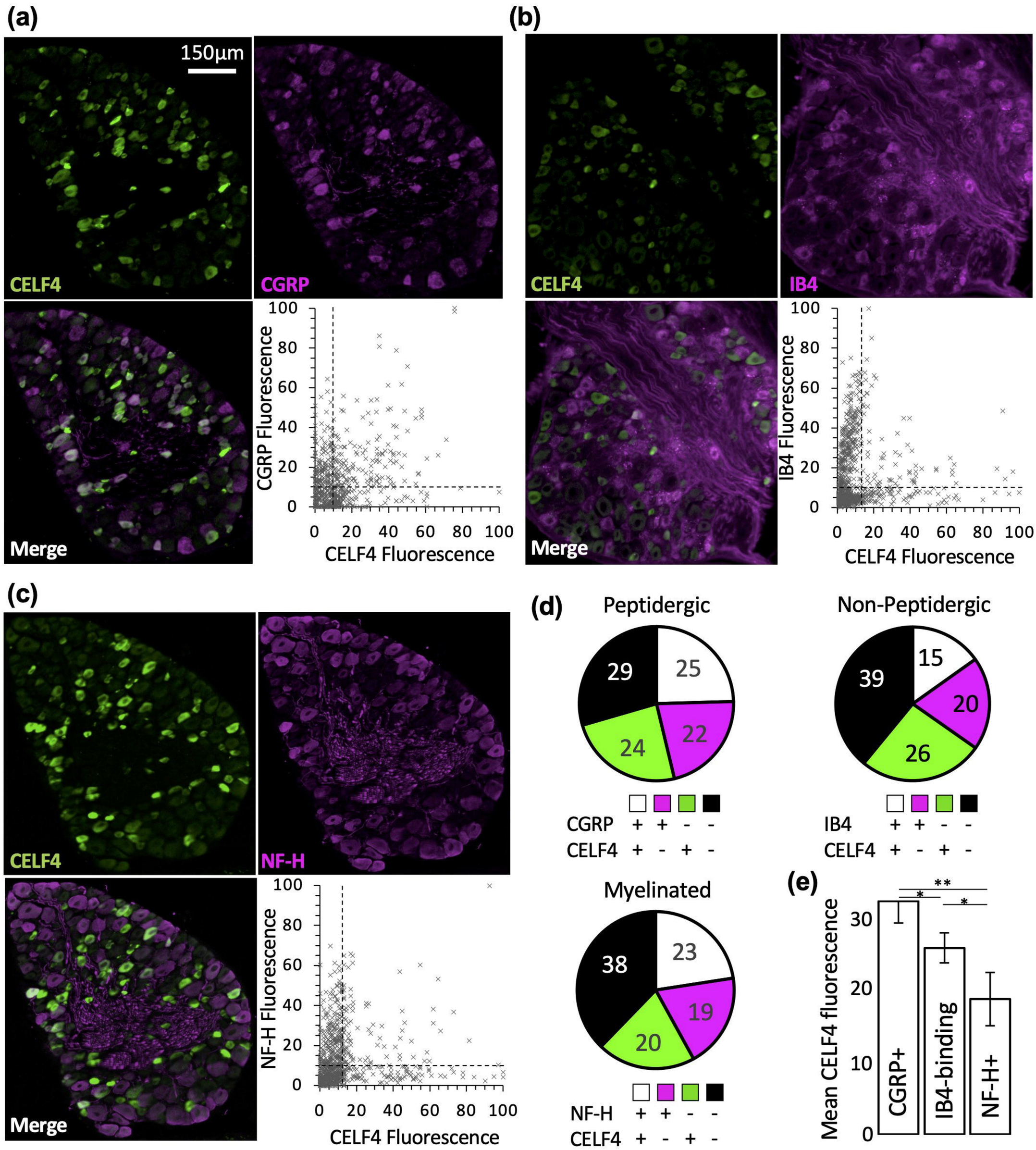
(a)
150µm
CELF4
CGRP
Merge
CGRP Fluorescence
CELF4 Fluorescence
(b)
CELF4
IB4
Merge
IB4 Fluorescence
CELF4 Fluorescence
(c)
CELF4
NF-H
Merge
NF-H Fluorescence
CELF4 Fluorescence
(d)
Peptidergic
29
25
24
22
CGRP + + - -
CELF4 + - + -
Non-Peptidergic
39
15
20
26
IB4 + + - -
CELF4 + - + -
Myelinated
38
23
19
20
NF-H + + - -
CELF4 + - + -
(e)
Mean CELF4 fluorescence
CGRP+
IB4-binding
NF-H+

Figure 5

(a)

mRNAs		*r*
CGRP vs NTRK1		**0.41**
CELF4 vs GFRA3		0.42
"	TRPV1	0.39
"	CALCA	0.34
"	TH	-0.11
"	MRGPRD	-0.09
"	NTRK3	-0.06
CGRP vs MRGPRD		**-0.05**

(b)

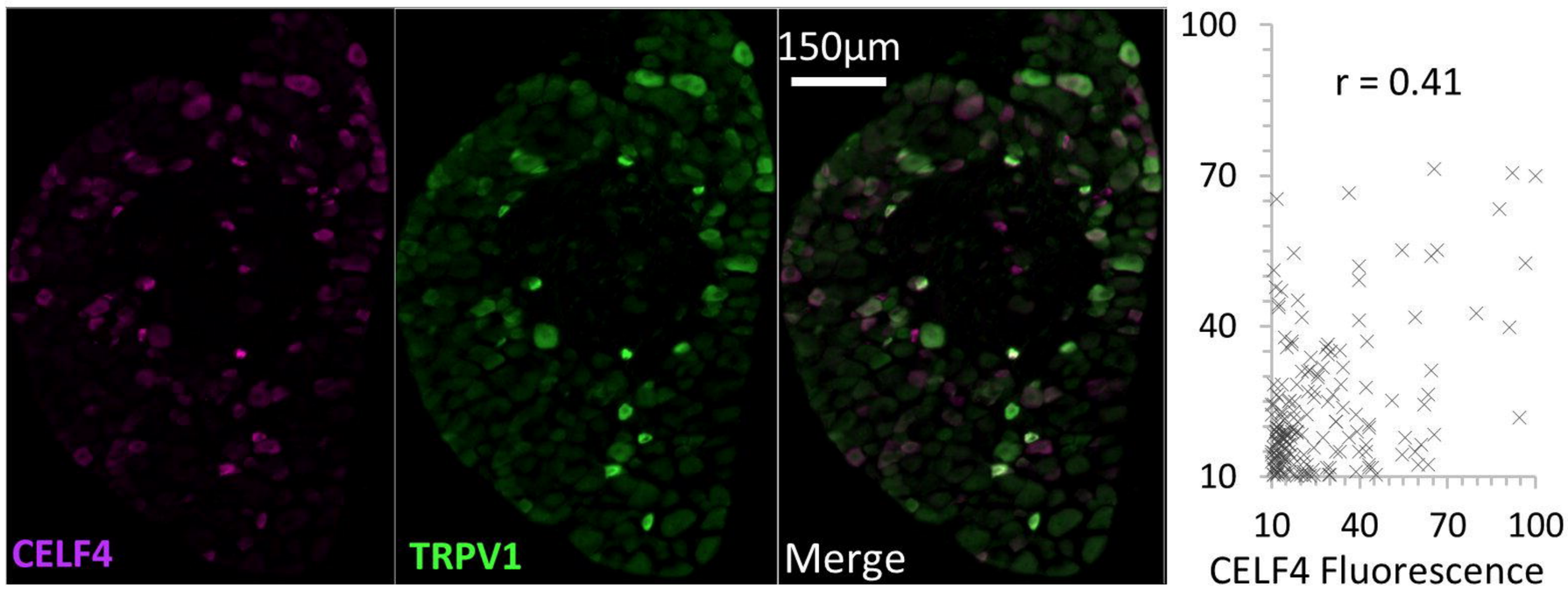

(c)

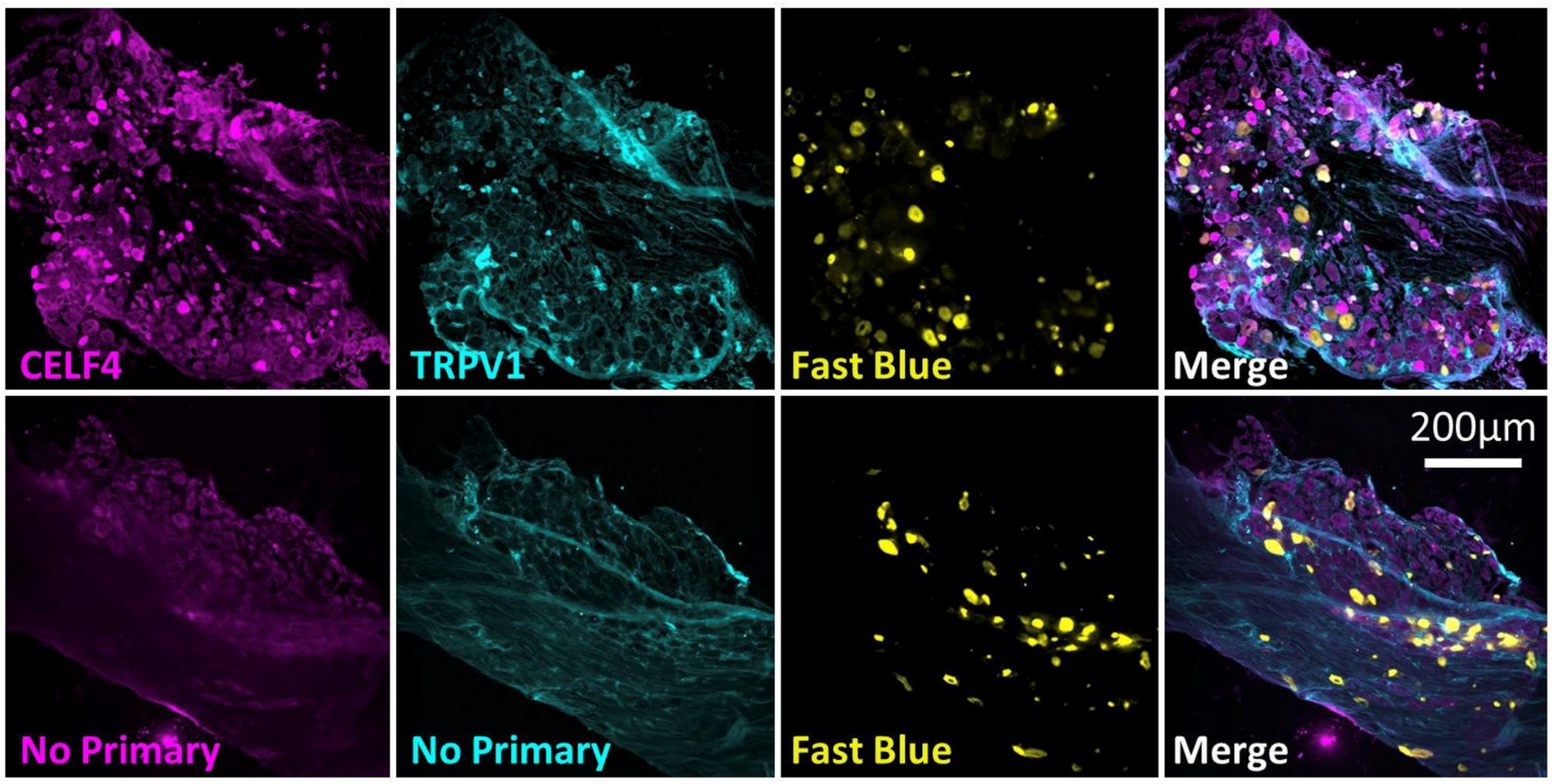

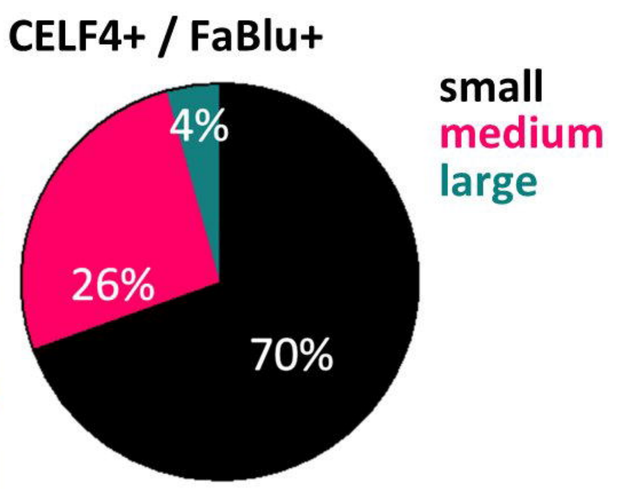

FaBlu+ that are TRPV1+: 41.9%
TRPV1+ that are CELF4+: 76.0%
CELF4+ that are TRPV1+: 49.8%

Figure 6

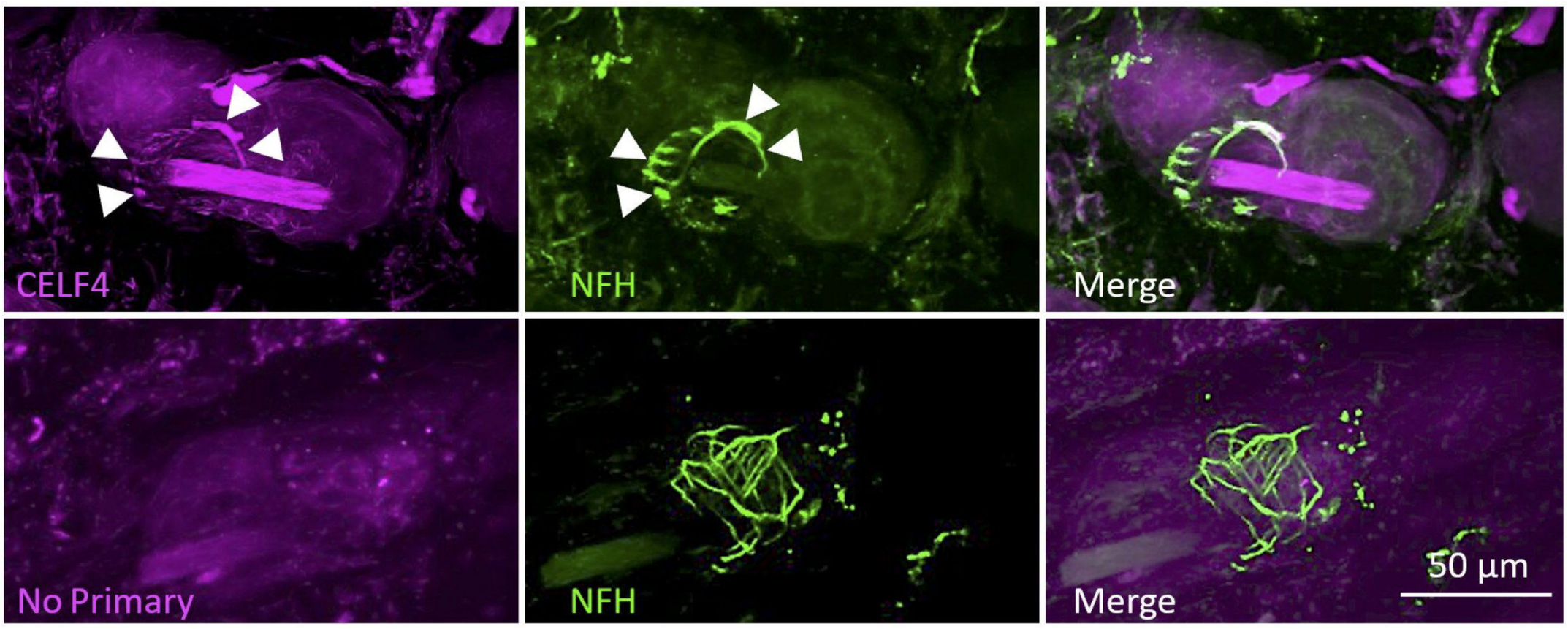

Figure 7

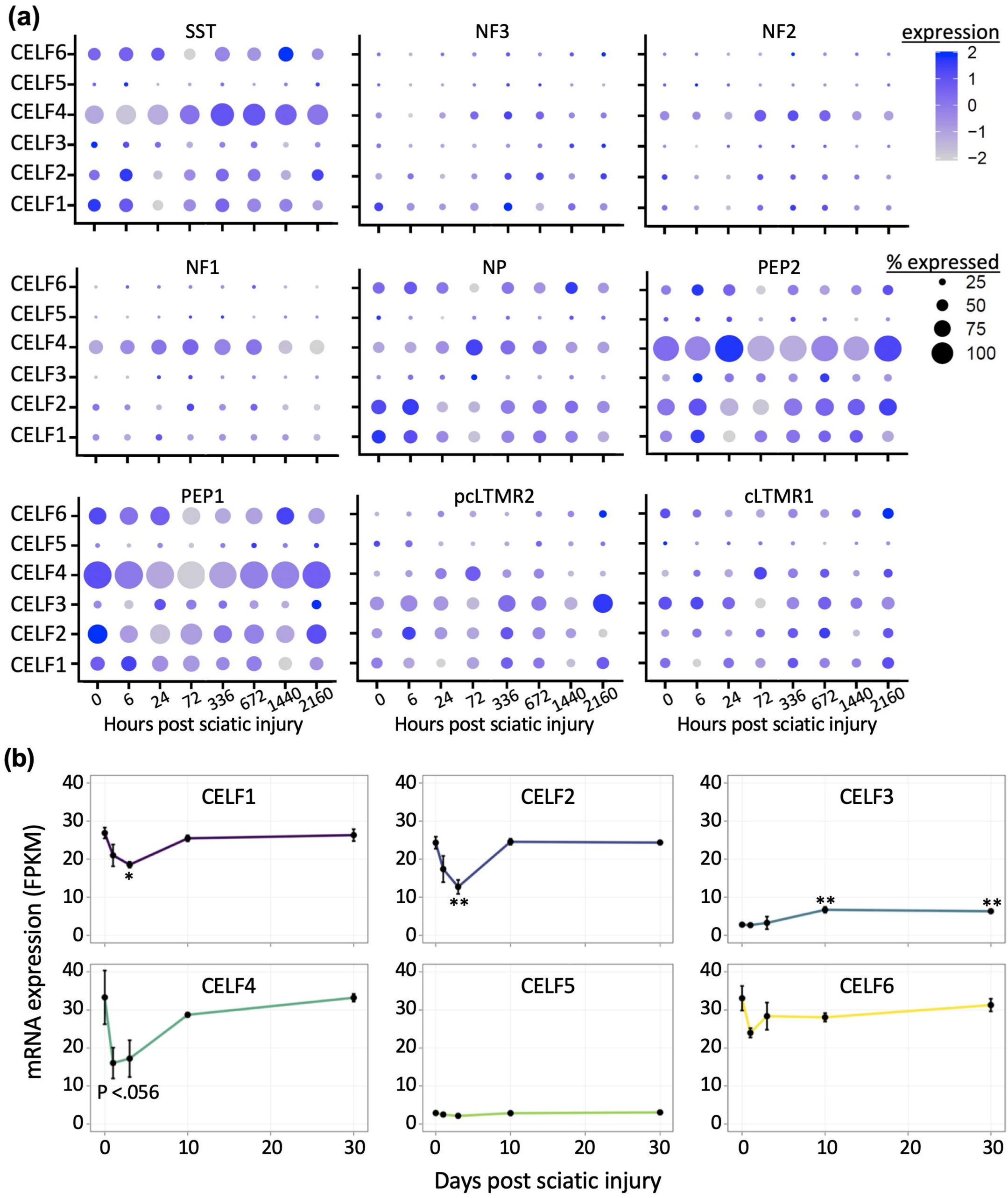
(a)
SST
NF3
NF2
NF1
NP
PEP2
PEP1
pcLTMR2
cLTMR1
CELF6
CELF5
CELF4
CELF3
CELF2
CELF1
expression
2
1
0
−1
−2
% expressed
25
50
75
100
0 6 24 72 336 672 1440 2160
Hours post sciatic injury
(b)
CELF1
CELF2
CELF3
CELF4
CELF5
CELF6
mRNA expression (FPKM)
P <.056
Days post sciatic injury

Figure 8

Target	*Immunogen*	*RRID*	*Host*	*Supplier*	*Cat #*	*Dilution Factor*
CELF4	MYIKMATLANGQA DNASLSTNGLGSSPG SAGHMNGLSHSPG NPSTIPMKDH	AB_10673035	Rabbit	Millipore Sigma	HPA037986	1:800
TRPV1	YTGSLKPEDAEVFKD SMVPGEK	AB_1624142	Guinea Pig	Neuromics	GP14100	1:500
NF-H	NF-H purified from bovine spinal cord	AB_2149761	Chicken	EnCor	CPCA-NF-H	1:40000
CGRP	ACDTATCVTHRLAGL LSRSGGVVKNNFVPT NVGSKAF	AB_1282813	Guinea Pig	Fitzgerald Industries International	20R-CP007	1:1500

Table 1: Primary antisera used for this study

Gene Ontology (GO) Term	*3'UTR-binding proteins (100)*	*Detected in DRG neurons (84)*	*Enriched in DRG neuron population(s) (17)*
posttranscriptional regulation of gene expression (GO:0010608)	8	8	1
regulation of mRNA metabolic process (GO:1903311)	33	32	8
regulation of translation (GO:0006417)	43	35	4
regulation of mRNA catabolic process (GO:0061013)	33	11	
regulation of mRNA stability (GO:0043488)	39	33	5
mRNA processing (GO:0006397)	45	43	10
RNA splicing (GO:0008380)	32	31	10
RNA localization (GO:0006403)	5	4	
regulation of gene silencing by miRNA (GO:0060964)	10	9	
RNA transport (GO:0050658)	10	7	1
cytoplasmic ribonucleoprotein granule (GO:0036464)	34	28	4
growth cone (GO:0030426)	6	6	2
dendritic spine (GO:0043197)	5	5	1
ribosome (GO:0005840)	6	6	2
distal axon (GO:0150034)	4	4	
nucleolus (GO:0005730)	16	16	1
dendrite (GO:0030425)	13	12	2
postsynaptic density (GO:0014069)	7	7	1
nuclear body (GO:0016604)	13	13	2
neuronal cell body (GO:0043025)	10	10	3
postsynapse (GO:0098794)	8	8	2

Table 2: Function of 3'UTR mRNA-binding proteins in populations of adult mouse sensory (DRG) neurons. 100 mouse genes are assigned the "3'UTR-binding" ontology term (Ashburner et al., 2000). mRNA's for 84 of these were detected in publicly available scRNA-Seq data derived from adult mouse DRG neurons (GSE59739, (Usoskin et al., 2015). 17 were significantly differentially expressed (FDR<0.05) between one or more of 4 DRG neuron populations (tyrosine hydroxylase–expressing, peptidergic, non-peptidergic, myelinated).

Gene	*Population*	*Average Enrichment*	*p*
CELF4	PEP	28.11	4.07E-12
CARHSP1	NP	15.76	8.95E-63
RBMS3	TH	5.52	4.68E-33
AUH	NF	3.64	1.67E-35
CELF6	PEP	2.98	2.25E-06
CELF6	NP	2.94	1.86E-20
CELF2	PEP	2.58	0.002704
CELF3	TH	2.53	1.35E-21
HNRNPA2B1	TH	2.21	1.65E-10
FXR2	NF	2.02	1.24E-14
ELAVL4	TH	2.02	5.72E-13
CSDC2	NF	1.93	1.37E-25
FXR2	NP	1.92	2.30E-05
RBMS1	NP	1.88	2.24E-13
RBFOX1	TH	1.78	0.000245
FXR2	PEP	0.56	0.006902
AUH	NP	0.46	0.003118
YBX3	NF	0.45	0.007494
TAF15	NF	0.40	2.32E-15
CELF6	NF	0.36	1.05E-07
CELF4	TH	0.31	1.38E-05
RBMS3	NP	0.29	3.77E-05
HNRNPL	NF	0.23	4.45E-05
RPS7	NF	0.20	0.000137
CARHSP1	NF	0.18	0.000383
CARHSP1	TH	0.17	3.98E-09

Table 3: 3'UTR mRNA-binding proteins significantly enriched (FDR<0.05) in DRG neuron populations, sorted by average fold enrichment. TH = tyrosine hydroxylase–expressing, NP = non-peptidergic, NF = neurofilament heavy chain-expressing and PEP = peptidergic neurons.

Family member	*Tissue Expression (Adult)*	*Subcellular Location*	*RNA-binding motif*	*Molecular/biological function(s)*
CELF1	Brain (m), spleen (m),liver(m), testis(m) ubiquitous(h)	Nuclear and cytoplasmic	UGUGUG,UGUU, CUGUCUG,UUGUG,	splicing,RNA stability, translation regulation (1-5)
CELF2	Brain (m), spleen (m),heart(m), lung(m),testis(m), ubiquitous(h)	Nucleoplasm, vesicles	UGUGU, UUGUU,UGUU,	RNA binding, mRNA processing,splicing
CELF3	Brain (m), adrenal gland (h),retina (h), pancreas (h)	Nucleus, cytoplasm	UGUUGUG (h)	RNA binding,mRNA splicing,spermatogenesis
CELF4	Brain (m,h), adrenal gland (h), retina (h)	Nucleus, cytoplasm, Axons/Dendrites	UGUGUKK(h), UGUGUGU*	RNA binding, mRNA processing, mRNA splicing
CELF5	Brain (m), N/A(h)	Nucleus, cytoplasm	UGUGUKK (h), UGUGUGU*	RNA binding
CELF6	Brain (m), N/A (h)	Nucleus, cytoplasm, synapse	UGUGKKG (h)	RNA binding, mRNA processing

Table 4: **CELF family RNA-binding protein tissue distribution, subcellular location, RNA recognition motifs and summarized function**. Tissue expression data from ProteomicsDB (Samaras et al., 2020; Schmidt et al., 2018). RNA-binding motifs were obtained from Transite (Krismer et al., 2020) and ATtRACT (Giudice et al., 2016) databases. * reported consensus sequence